CENP-E initiates chromosome congression by opposing Aurora kinases to promote end-on microtubule attachments close to centrosomes

Kruno Vukušić*, Iva M. Tolić*

Division of Molecular Biology, Ruđer Bošković Institute, Zagreb, Croatia

*Corresponding authors

E-mail: kvukusic@irb.hr, tolic@irb.hr

SUMMARY

Chromosome congression to the spindle equator, which recurrently fails in cancer cells leading to aneuploidy, requires the kinetochore motor protein CENP-E/kinesin-7. Current models state that chromosomes congress by CENP-E-driven gliding along spindle microtubules. Here, we show that CENP-E is not essential for the congression movement, but for initiating movement through the formation of end-on attachments. We reached this conclusion by large-scale live-cell imaging under varying activity of CENP-E using lattice light-sheet microscopy. We found that congression without CENP-E is delayed by the activity of centriole-dependent Aurora A and outer-kinetochore-localized Aurora B kinases, which limit the formation of end-on attachments. CENP-E bypasses this inhibition by causing a decrease in Aurora B activity and in phosphorylation of its outer-kinetochore targets. Chromosomally unstable cancer cells rely on CENP-E more than non-cancer cells, leading to segregation errors specifically in cancer cells with prolonged mitosis, thereby exposing a mitotic timing-dependent vulnerability of cancer cells.

INTRODUCTION

To segregate equally into the two daughter cells, duplicated chromosomes achieve biorientation by connecting to microtubules extending from the opposite spindle poles, which satisfies the spindle assembly checkpoint (SAC)[1–3]. Chromosomes positioned close to one spindle pole, termed polar chromosomes, show a characteristic movement from the pole to the equatorial region of the spindle during early mitosis, termed chromosome congression[4]. Chromosomes that fail to congress during prometaphase prolong mitosis by activating SAC[5] and contribute to chromosomal instability in cancer cells[6–8]. Polar chromosomes are particularly prone to alignment failure during erroneous mitosis[8] and these chromosomes exclusively require the activity of the kinetochore motor protein Centromere-associated protein E (CENP-E/kinesin-7) for congression[4]. Thus, CENP-E-mediated congression seems to be peculiar in both its dynamics, signaling, and final efficiency, leaving chromosomes that must take this route to alignment in particular danger during erroneous mitosis in cancer cells[9].

CENP-E function during early mitosis has been studied extensively[1,4,10–21]. The most prominent model of CENP-E function states that CENP-E glides polar kinetochores that are attached laterally to microtubules independently of biorientation by its microtubule plus-end directed motor activity[22–24]. The preference for CENP-E in a tug of war with the minus-end directed kinetochore motor dynein was explained by a single-site (T422) phosphorylation of CENP-E by Aurora kinases close to the spindle poles[25] and tubulin detyrosination of kinetochore fibers[26], both of which favor the activity of CENP-E[27,28]. Other CENP-E functions include the establishment of lateral attachments[11], formation of antiparallel microtubule bundles[29], microtubule tip-tracking[21,30], and sorting of microtubules nucleated from kinetochores[31], all as a component of a large crescent-shaped structure of the outer kinetochore known as the fibrous corona that sheds from the kinetochore upon establishment of stable end-on attachments[15,28]. However, chromosome congression in the absence of CENP-E was observed in several studies[4,12,25,31–33], which contradicts the prevailing model. Thus, the mechanism of chromosome congression and the function of CENP-E in this process remains unclear.

Here, we uncovered that congression consists of two steps, initiation and movement, and that CENP-E is required specifically for the initiation of congression by triggering the formation of end-on attachments, instead of driving the movement itself. This finding is in contrast with the current model[19], but instead consistent with pioneering models in which congression requires biorientation[34]. We arrived at this conclusion by developing a large-scale live-cell imaging strategy using lattice light-sheet microscopy (LLSM), which allowed us to simultaneously observe hundreds of cells as their chromosomes undergo congression. In combination with reversible chemical inhibitions of multiple targets implicated in congression, this strategy enabled us to systematically test in a time-resolved manner the hierarchy of molecular networks operating during congression. We uncovered that CENP-E initiates the formation of end-on attachments, a crucial first step of congression, by observing both gradual decrease of SAC proteins on kinetochores and gradual formation of end-on attachments. We uncover that congression operates as a negative feedback loop between the activity of Aurora kinases that oppose congression by destabilizing end-on attachments near the spindle pole, but also activate CENP-E, which then promotes

congression by opposing the activity of Aurora kinases. Finally, we show that chromosomally unstable cancer cells are drastically less efficient in chromosome congression after perturbation of CENP-E compared to non-cancer cells, leading to reduced mitotic fidelity and aneuploidy specifically in cancer cells with prolonged mitosis. Our findings suggest that the sensitivity to chromosome congression problems in prolonged mitosis, which is enhanced in tumor cells, could be exploited in the development of new anti-tumor strategies.

RESULTS

CENP-E is essential only for the initiation of movement of polar chromosomes during congression

To uncover the molecular mechanisms of chromosome congression, we developed an assay for systematic testing of the role of specific molecular players in this process. We used CENP-E inactivation or depletion (referred to jointly as CENP-E perturbation), which results in fully formed spindles with two populations of chromosomes: those aligned at the spindle midplane and polar chromosomes "synchronized" at a location close to the spindle poles[4]. We then studied the movement of polar chromosomes, which were uniform in both their initial positions and the distance they had to travel to reach the spindle midplane, thereby avoiding variabilities between chromosomes occurring in normal mitosis[35]. To image simultaneously hundreds of individual cells (1.5 mm field of view) in complete volumes (35 μm depth) with high spatiotemporal resolution (~350 nm and 2 min/image) for a prolonged duration (24 hours), we established a live-cell imaging approach based on lattice light-sheet microscopy (Fig. 1A, Video S1, see Fig. S1 for comparison with confocal microscopy). This approach produced a live-cell movie library of the non-transformed human cell line RPE-1 under four different conditions: 1) "CENP-E reactivated", obtained by reactivating CENP-E motor activity after its inhibition by the small-molecule inhibitor GSK923295[36] and subsequent wash-out, 2) "CENP-E depleted", obtained by depletion of CENP-E by the use of small interfering RNAs (siRNAs), 3) "CENP-E inhibited", obtained by continuous inhibition of CENP-E by GSK923295, and 4) "control", treated just with DMSO (Fig. 1B).

We reasoned that the movement of polar chromosomes would be different in the presence or absence of CENP-E activity if chromosome congression is driven by CENP-E, or similar if CENP-E is involved in other processes essential for congression, but not the movement itself (Fig. 1C). Following reactivation of CENP-E, all polar chromosomes successfully congressed to the metaphase plate during 60 min (Fig. 1D, S1A, Video S2). Furthermore, polar kinetochores approached the equatorial region in a highly uniform manner, characterized by initial slower and faster second phase of movement (Fig. 1D, S1A)[19], gradual increase in interkinetochore distance (Fig. S1B), and a gradual reorientation of the axis between sister kinetochores toward the main spindle axis (Fig. S1C), similar to kinetochores during early prometaphase in control cells (Figs. 1D, S1A-C, Video S2)[35] although slower phase of congression was not observed in control cells (Fig. 1D). We thus conclude that the CENP-E-driven congression of polar chromosomes after CENP-E reactivation recapitulates the main features of their congression during prometaphase.

In CENP-E depleted and CENP-E inhibited conditions, the number of polar chromosomes decayed gradually after the onset of mitosis as chromosomes congressed to the metaphase plate (Fig. 1D, Video S3)[37]. Due to the large number of cells imaged by our LLSM assay, we were able to follow the dynamics of numerous polar kinetochores that successfully completed alignment in both depleted CENP-E (Figs. 1A, D, S1D, Video S3) and CENP-E inhibited cells (Fig. 1D, Video S3). Intriguingly, the movement of polar kinetochores toward the plate was highly similar between conditions with active and perturbed CENP-E (Fig. 1D), and was accompanied by an increase in interkinetochore distance and reorientation of the kinetochore pair towards the spindle axis in all conditions (Figs. 1D, S1A-D). Furthermore, the mean velocities of sister kinetochore movement

during 6 minutes before joining the plate, which corresponds to the major part of the congressional movement (Figs. 1D, S1A-D), were indistinguishable between conditions (Fig. 1E). This implies that polar chromosomes move from the spindle poles to the equator in a manner independent from the activity of CENP-E, arguing against models where CENP-E moves polar chromosomes by gliding along spindle microtubules.

Although congressional movement was highly similar with and without CENP-E activity, in the CENP-E perturbed conditions less than 20% of polar kinetochores initiated congression in a 30 min period following the end of prometaphase spindle elongation compared to more than 70% in the CENP-E reactivated and 100% in control condition (Figs. 1D, F, S1A-D, Videos S2 and S3), implying a role of CENP-E in the initiation of kinetochore movement. As the congression of polar chromosomes in the absence of CENP-E activity occurs over a prolonged period after the onset of mitosis (Fig. 1D, Video S2 and S3), we tested whether the dynamics of congression changes with the time spent in mitosis. There was no correlation between the velocity of congression and the time elapsed from the onset of mitosis until the congression event across conditions (Fig. S1E), suggesting that the dynamics of chromosome movement during congression is robust to the time spent in mitosis. To conclude, we show that CENP-E is not crucial for the congression movement of polar chromosomes, but that CENP-E is instead critical for initiating this movement.

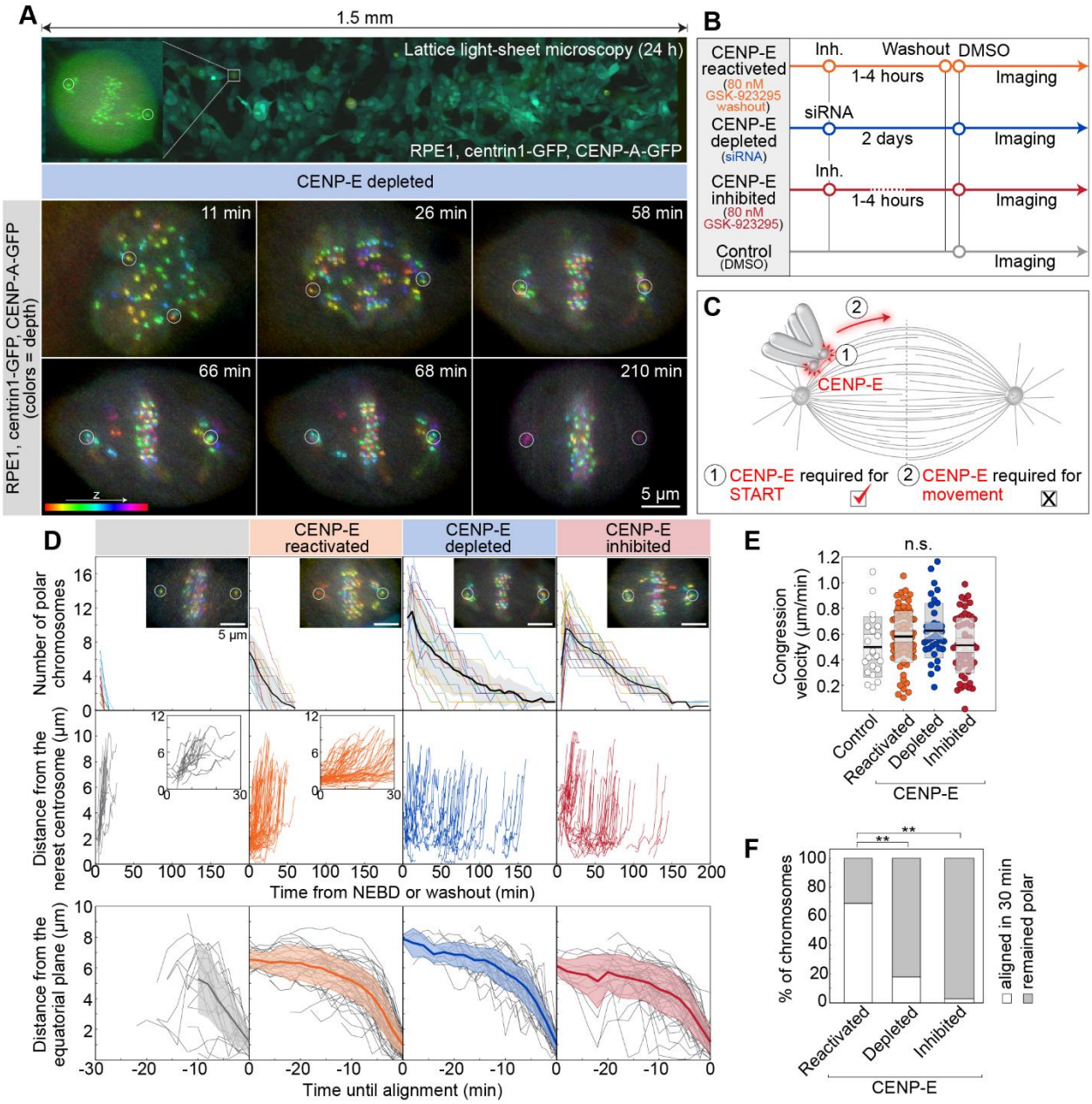

Figure 1. CENP-E activity is required only for rapid initiation and not for the movement of polar chromosomes during congression. (A) Field of imaging 1.5mm wide that includes dozens of RPE-1 cells expressing centrin1-GFP (white circles) and CENPA-GFP imaged by lattice light sheet microscopy (LLSM). Cells were treated with the 80 nM CENP-E inhibitor GSK-923295 for 3 h prior to imaging. The small area with one mitotic cell on a large field depicted with a square is zoomed in on the left (top). Example of a representative RPE-1 cell undergoing mitosis after CENP-E depletion imaged using the LLSM assay on top. The images are a maximum projection color coded by depth as specified by the color bar. Time 0 represents the onset of mitosis. (B) Scheme of the protocol to obtain varying and acutely controllable levels of CENP-E activity in cells. (C) Scheme depicting the hypothesis that CENP-E, depicted by red glow signs, is required for the initiation of chromosome congression (START), depicted by 1, or for the movement of chromosome during congression, depicted by 2. The tick represents the interpretation favored by the results obtained. (D) Number of polar chromosomes in time over different treatments,

depicted in different colors (top). Distance from the nearest pole of the kinetochore pairs in time from nuclear envelope breakdown (NEBD) or washout time for CENP-E reactivated with enlargements of data over the x-axis in the upper right part (middle). Distance from the equatorial plane of pairs of kinetochores over time until alignment in different treatments. Thick lines represent means, and the grey areas over means represent standard deviations. (E) Velocity of chromosome congression during the 6-minute period that precedes alignment for depicted treatments. The black line shows the mean; the light grey and dark grey areas mark the 95% confidence interval on the mean and standard deviation, respectively. Numbers: control (15 cells, 32 kinetochore pairs), reactivated (18 cells, 86 kinetochore pairs), CENP-E depleted (18 cells, 69 kinetochore pairs), inhibited (12 cells, 65 kinetochore pairs), each from at least three independent experiments. (Statistics: (F) Frequency of pairs of kinetochores that aligned (white) or remained polar (grey) during the 30-minute period in the indicated treatments. One-way ANOVA (n.s., non-significant, $*p < 0.05$; $**p < 0.01$; $***p < 0.001$; $****p < 0.0001$). Inh., inhibitor, siRNA, small interfering RNA.

CENP-E on polar kinetochores initiates the conversion of lateral to end-on attachments to microtubules

We hypothesized that CENP-E plays a role in the establishment of end-on microtubule attachments[11,38–41] of polar kinetochores, which we assumed to be a crucial event for the initiation of chromosome congression. To explore this hypothesis, we reactivated CENP-E in cells expressing the SAC protein Mad2, which accumulates on kinetochores lacking end-on attachments[42–44], to track over time the response of kinetochore-microtubule attachments to CENP-E reactivation. Immediately after CENP-E reactivation, polar kinetochores had high levels of Mad2, indicating the absence of end-on attachments (Figs. 2A, S2A)[4]. As a response to CENP-E reactivation, Mad2 levels on polar kinetochores gradually decreased over time (Figs. 2A, B, S2A, Video S4), in contrast to the cells in which CENP-E was continuously inhibited and Mad2 levels remained constant (Fig. 2SB). Interestingly, the loss of Mad2 on polar kinetochores started, on average, prior to their movement towards the equatorial plane (Figs. 2B, S2C, D). During congression, Mad2 levels did not show a tendency to be higher on either the sister kinetochore closer to the spindle pole or the one further away from the pole (Fig. S2E), suggesting that near the pole both sister kinetochores have a similar chance of initiating end-on conversion following CENP-E reactivation. These results imply that the formation of end-on attachments on polar kinetochores depends on CENP-E and occurs before the congression movement of the kinetochores.

The average Mad2 signal on sister kinetochores after CENP-E reactivation was higher at the kinetochore pairs that were closer to the spindle pole, and most kinetochores approached the metaphase plate with Mad2 signal intensities indistinguishable from those of aligned kinetochores (Fig. 2C). The Mad2 signal was negatively correlated with the distance between sister kinetochores, which serves as a readout of inter-kinetochore tension (Fig. S2F). These results imply that after CENP-E reactivation polar kinetochores gradually acquire end-on attachments, which are able to generate tension on the kinetochores. The speed of kinetochore movement after CENP-E reactivation was correlated with the rate of Mad2 loss (Fig. 2D). In agreement with this, kinetochore pairs that aligned within 30 minutes after CENP-E reactivation lost Mad2 faster compared to those that remained polar (Fig. S2C, D). This suggests that the speed of congression

is dictated by the rate of formation of end-on attachments, which is reflected in the rate of Mad2 loss.

To directly observe and quantify different types of microtubule attachments to kinetochores during chromosome congression, we performed super-resolution imaging of spindle microtubules by using Stimulated Emission Depletion (STED) microscopy in CENP-E inhibited cells (Fig. 2E). As expected, the majority (~70%) of polar chromosomes had both sister kinetochores laterally attached to the microtubules (Fig. 2E, F, S2G). Interestingly, ~25% of polar chromosomes contained mixed lateral and end-on attachments, and only ~5% of polar chromosomes contained end-on attachments on both sister kinetochores similar to the kinetochore pairs aligned at the metaphase plate (Fig. 2E, F, S2G). These attachment states showed a gradual increase in inter-kinetochore distance (Kuhn and Dumont, 2017), with the smallest distance for laterally attached kinetochores and the largest for the bioriented pairs (Fig. 2G). Thus, our super-resolution images provide direct visualization of the conversion from lateral kinetochore-microtubule attachments, which lack significant tension, to the load-bearing end-on attachments. To conclude, these results imply that CENP-E is crucial for the first steps of lateral to end-on conversion of kinetochore attachments to microtubules (Fig. 2H), inducing a drop in Mad2 levels and instigating congression movement that does not depend on CENP-E.

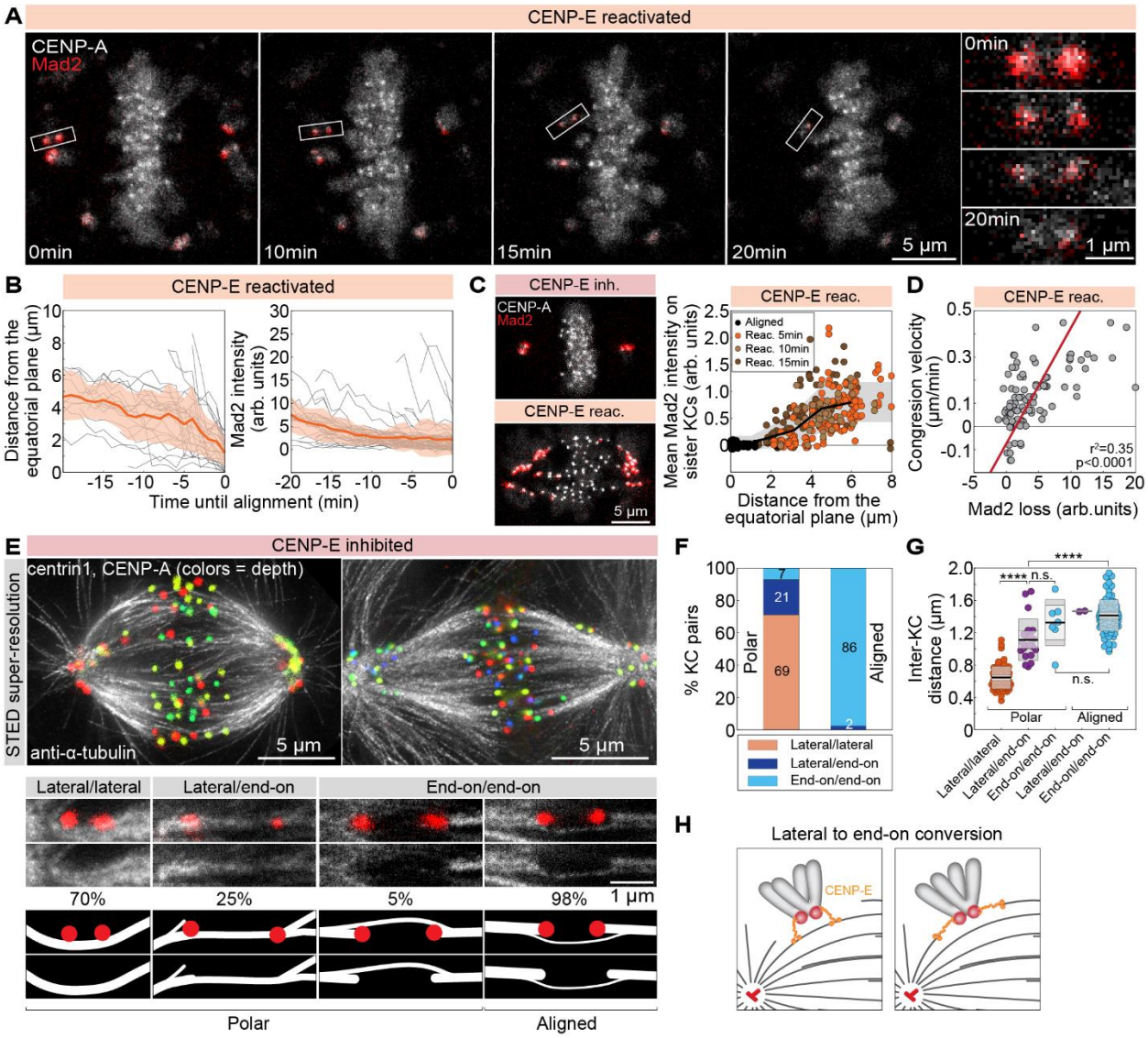

Figure 2. Initiation of chromosome congression after CENP-E reactivation is accompanied by lateral to end-on transition of microtubule attachments to kinetochores. (A) Representative examples of a cell expressing Mad2-mRuby (red) and CENPA-mCerulean (grey) in different times after the washout of the CENP-E inhibitor as depicted. Images on the right are enlargements of sister kinetochores during congression, as per boxed area on the left. Time 0 represents the washout of the CENP-E inhibitor. (B) Distance of pairs of kinetochores from the equatorial plane (left) and mean Mad2 intensity on of kinetochore pairs (right) in time until alignment. (C) Representative examples of cells expressing Mad2-mRuby (red) and CENPA-mCerulean (grey) fixed in the presence of CENP-E inhibitor (top) or 5 minutes after the washout of the inhibitor (bottom) (left). Distance of kinetochore pairs from the metaphase plate over the mean Mad2 signal intensity of kinetochore pairs under indicated conditions. Thick line represent mean for binned data values, and the grey area over the mean represents the standard deviation of a mean for binned data (right). (D) Congression velocity during 30-min period after CENP-E inhibitor wash-out over loss of Mad2 signal intensity in kinetochore pairs and linear regression (line). (E) Representative

examples of two spindles immunostained for α-tubulin and imaged by stimulated emission depletion (STED) microscopy in cells expressing CENP-A-GFP and centrin1-GFP. Projection is color coded by depth as specified by the color bar in 1A (top). Insets of kinetochore pairs with microtubules from different attachment categories, as depicted, and schemes of microtubules (white) and kinetochores (red) of the respective insets. The percentages represent the frequency of different attachment categories (bottom). (F) Frequency of indicated attachment categories in the indicated groups. (G) Interkinetochore distances for indicated microtubule attachment categories across spindles treated with the CENP-E inhibitor. The black line shows the mean; the light and dark gray areas mark 95% confidence intervals on the mean and standard deviation, respectively. (H) Scheme depicting the model based on obtained results in which CENP-E is crucial for rapid lateral-to-end-on conversion close to the spindle pole. All images are a maximum projection of all acquired z planes. Numbers: B, D (14 cells, 54 kinetochore pairs), C (26 cells, 135 kinetochore pairs), F, G (20 cells, 185 kinetochore pairs), each from at least three independent experiments. Statistics: unpaired t-test (n.s., non-significant, $*p < 0.05$; $**p < 0.01$; $***p < 0.001$; $****p < 0.0001$). arb., arbitrary, inh., inhibited, reac., reactivated.

Aurora kinases prevent chromosome congression in the absence of CENP-E activity

Having identified that CENP-E promotes end-on attachments to initiate congression, we set out to systematically test in a time-resolved manner the hierarchy of molecular networks operating during this process. We took advantage of our methodological advance achieved by using lattice light-sheet microscopy and combined it with reversible chemical inhibitions of multiple targets implicated in congression (Fig. 3A)[1]. First, we hypothesized that in the absence of CENP-E congression is prevented by a molecular signaling cascade that delays the formation of end-on attachments, which means that if end-on conversion is induced independently of CENP-E, this should result in congression of polar chromosomes. We started with inhibition of Aurora B kinase, as it was shown in monopolar spindles that its removal constitutes an essential step for the lateral to end-on transition[45] and the removal of the Mad1:Mad2 complex from kinetochores[32,45]. Fascinatingly, after acute inhibition of aurora B by 3µM ZM-447439[46] in both CENP-E-inhibited and depleted conditions, polar chromosomes immediately started moving and most of them completed congression within 30 minutes after the addition of the inhibitor (Figs. 3B-D, S3A-F, Video S5), while a small fraction ended the journey close to the metaphase plate (Figs. 3B, S3F). These results imply that polar chromosomes initiate congression instantly without CENP-E if end-on conversion is allowed by the acute inhibition of Aurora B.

Chromosome congression after acute inhibition of Aurora B in the absence of CENP-E activity was not dependent on the premature onset of anaphase[47] (Fig. S3G), concentration (Fig. S3H), nor specificity of Aurora B inhibitor[48] (Fig. S3I). Furthermore, the depletion of the cohesion release factor WAPL[49] (Fig. S3J), the co-depletion of the chromokinesins Kid/kinesin-10 and Kif4a/kinesin-4[4] (Figs. 3C, S3K), nor the inhibition of PP1/PP2A phosphatase activity by Okadaic acid[50] (Figs. 3C, S3K, L) did not stop chromosomes from initiating and finishing congression after acute inhibition of Aurora B in the CENP-E inhibited condition. This implies that the loss of centromeric cohesion[51], the polar ejection forces generated by chromokinesins on chromosome

arms[38,52] and the activity of phosphatases[53] are not essential for congression movements after acute inhibitions of Aurora B and CENP-E. Intriguingly, chromosome congression without CENP-E and Aurora B activities was characterized by fast movement of polar kinetochores toward the equatorial plane, gradual increase in interkinetochore distance, and gradual reorientation toward the spindle axis, similar to CENP-E reactivation (Fig. S1A), but it distinctively lacked the slower first phase of congression (Fig. S3A-B). This suggests that only the slower first phase of congression after CENP-E reactivation depends on Aurora B activity, implying that the role of CENP-E in chromosome congression may be through the down-regulation of Aurora B activity.

To gain further insight into signaling that limits chromosome congression in the absence of CENP-E, we co-inhibited or depleted various molecular regulators that are involved in the regulation of biorientation or Aurora B recruitment[54] under CENP-E inhibited condition. Interestingly, co-inhibition of Aurora A kinase, which shares specificity and certain kinetochore targets with Aurora B, most notably Highly expressed in cancer 1 (Hec1)[55], induced congression of polar chromosomes although much slower than acute aurora B inhibition (Figs. 3B-D, Video S5). On the other hand, neither inhibition nor co-inhibition of Budding uninhibited by benzimidazoles 1 (Bub1) or Haspin, factors essential for the recruitment of Aurora B to the outer and inner centromere, respectively[56–59], were able to induce chromosome congression in the absence of CENP-E, as well as inhibition of Monopolar spindle 1 (Mps1) kinase, Polo-like kinase 1 (Plk1) kinase, and depletion of Bub1-related (BubR1) pseudokinase (Figs. 3C, S3M). This implies that of the tested kinases, only Aurora A and the outer-kinetochore localized Aurora B limit the initiation of congression in the absence of CENP-E.

Perturbations of microtubule motor proteins and crosslinkers revealed that neither indirect, by removing Spindly[60,61], nor direct[62] perturbation of dynein activity at kinetochores induced congression of polar chromosomes in the absence of CENP-E, similar to the depletion of the crosslinker of antiparallel microtubules PRC1[63,64], co-depletion of the chromokinesins Kid and Kif4a, and acute inhibition of Eg5/kinesin-5 that results in spindle shortening (Figs. 3C, S3M, N). These results suggest, respectively, that the poleward pulling forces exerted by kinetochore dynein, the thickness of antiparallel microtubule bundles to which kinetochores are initially laterally attached[29], the activity of chromokinesins, and the distance between the plus ends of microtubules nucleated in one spindle half and the opposite spindle pole are not major obstacles to congression in the absence of CENP-E activity. Instead, the primary barrier to congression without CENP-E is the activity of Aurora kinases.

CENP-E initiates congression by triggering lateral to end-on conversion in a manner dependent on BubR1, but independent of phosphatases

We next used the CENP-E reactivated condition to test which molecular factors regulate chromosome congression upstream and downstream of CENP-E in a time-dependent manner (Fig. 3E). As a first hypothesis, we assumed that the role of CENP-E in the initiation of chromosome congression reflects the recruitment of Protein phosphatase 2A (PP2A) to the outer kinetochore, either directly or through its interaction with BubR1[25,65]. However, acute inhibition of PP1/PP2A activities by Okadaic acid did not prevent chromosome congression after reactivation of CENP-E (Figs. 3F-H, S4A, Video S5), similarly to the finding that inhibition of PP1 phosphatase in HeLa

cells during prometaphase did not block congression of polar chromosomes[25]. Congression after CENP-E reactivation was also successful without the activities of Plk1 kinase, Kif18a/kinesin-8, which promotes chromosome alignment at the metaphase plate[66], or the chromokinesins Kid and Kif4a and thus the polar ejection forces they generate[38] (Figs. 3G, S4B).

Phosphorylation of CENP-E mediated by Aurora kinases was previously reported to be required for the motor activity of CENP-E during congression[25]. However, polar chromosomes were able to congress after reactivation of CENP-E when Aurora B kinase was acutely inhibited (Figs. 3G, S4C, D). Similar to the acute inhibition of Aurora B in the absence of CENP-E activity (Fig. 3B-D), congression after acute inhibition of Aurora B in the presence of CENP-E activity was occasionally characterized by an incomplete congression of polar chromosomes (Fig. S4D), suggesting that problems in error correction that are the result of Aurora B inhibition[67], limit complete congression of polar chromosomes. To sum up, polar chromosomes can initiate congression when total Aurora B is inhibited, regardless of CENP-E activity.

To understand whether CENP-E activity can promote congression when end-on attachments are either prematurely stabilized or prevented, we performed two sets of experiments. First, we reactivated CENP-E in cells depleted of Spindly, a kinetochore adaptor of dynein[61], which contain an increased number of polar chromosomes with stabilized end-on attachments[4]. The percentage of polar chromosomes that congressed after reactivation of CENP-E was significantly reduced in Spindly-depleted cells when compared to controls (Figs. 3G, S4E), suggesting that CENP-E is less efficient in initiating congression of polar chromosomes with stable end-on attachments that are often found behind the spindle pole and/or Spindly depletion reduces CENP-E levels on kinetochores[68]. Second, the movement of polar chromosomes in Hec1-depleted cells, which lack the ability to form end-on attachments[69], did not depend on CENP-E activity, as the chromosomes moved in a similar manner in Hec1-depleted cells and Hec1-depleted and CENP-E-inhibited cells (Fig. S4F), similar to previous reports in HeLa cells[33]. These results imply that CENP-E cannot promote congression when end-on attachments are prematurely stabilized or cannot be formed.

Lastly, we tested the requirement for BubR1 during CENP-E-mediated congression of polar chromosomes. We depleted BubR1 and inhibited CENP-E together with MG132 treatment to prevent the premature onset of anaphase[70]. Surprisingly, when we reactivated CENP-E in BubR1-depleted cells, the congression of polar chromosomes was almost completely blocked (Fig. 3F-H, Video S5). We conclude that BubR1 is crucial for the lateral to end-on conversion and the subsequent chromosome congression, likely by phosphorylating CENP-E[41], and/or by recruiting CENP-E to kinetochores[71].

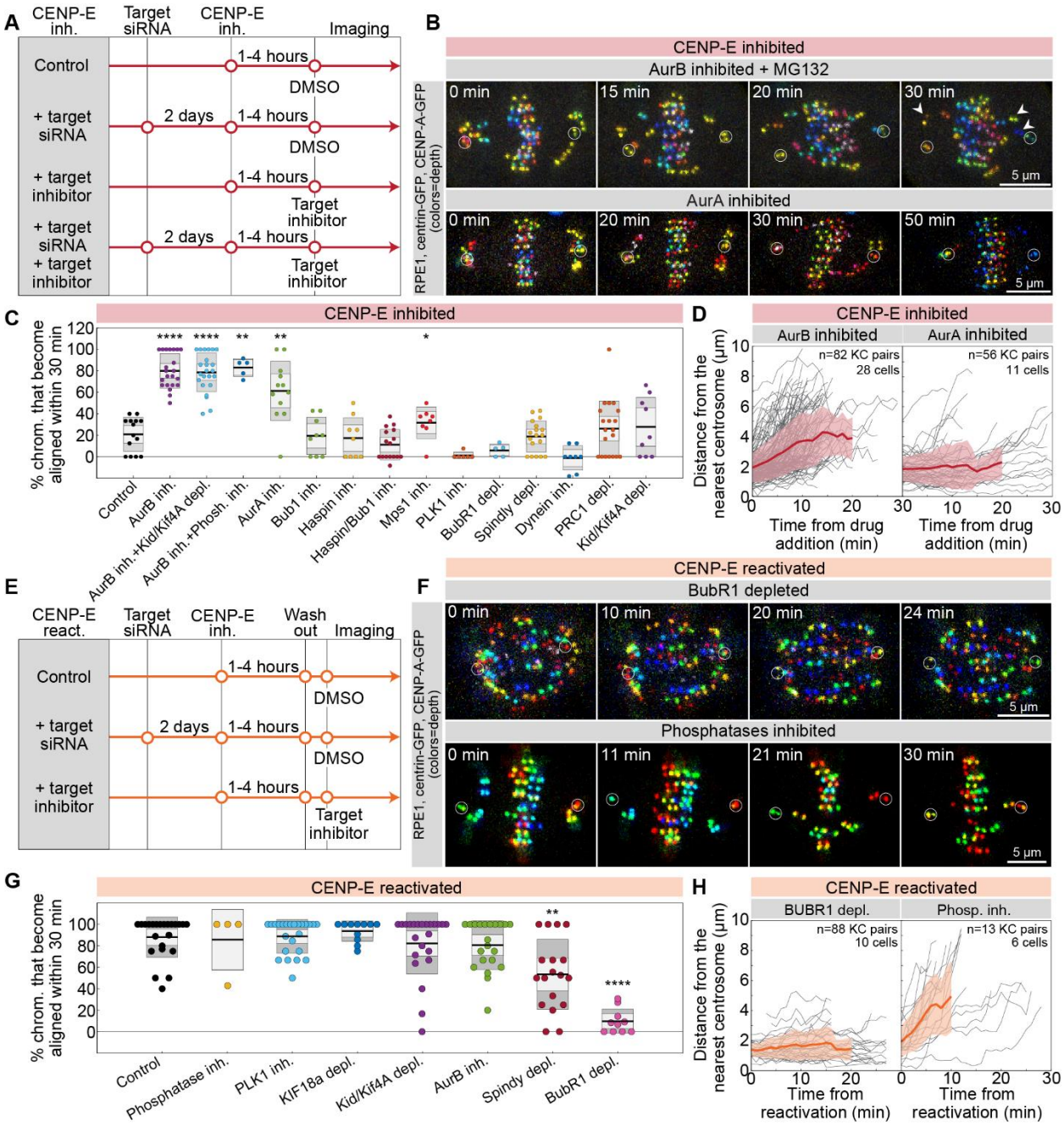

Figure 3. Aurora kinases limit congression without CENP-E, while lateral attachments and BubR1 are prerequisites for CENP-E-mediated congression. (A) Scheme of the experimental protocol to test which molecular factors limit chromosome congression in the absence of CENP-E activity. (B) Representative examples of cells expressing CENP-A-GFP and centrin1-GFP (denoted by white circles) in the presence of CENP-E inhibitor at different times after acute inhibition of target proteins as depicted. Time represents the time from drug treatments. (C) Frequency of polar chromosomes that aligned in the 30-minute period after indicated treatments in the presence of CENP-E inhibitor. The black line shows the mean; the light and dark grey areas mark the 95% confidence interval on the mean and standard deviation, respectively. Numbers of

cells per treatment: 14, 22, 23, 5, 12, 9, 9, 17, 8, 6, 5, 18, 8, 20, 9, each from at least three independent experiments. (D) Distance to the nearest centrosome in time from the indicated acute treatment. Thick lines represent means, and gray areas over means represent standard deviations. (E) Scheme of the experimental protocol to test which molecular factors regulate the congression of polar chromosomes after the reactivation of CENP-E activity by the wash-out of the CENP-E inhibitor. (F) Representative examples of cells expressing CENP-A-GFP and centrin1-GFP at different times after acute inhibition of the depicted targets following wash-out of the CENP-E inhibitor. Time represents the time from wash-out. (G) Frequency of polar chromosomes that aligned in the 30-minute period after the wash-out of the CENP-E inhibitor in the indicated treatments. Numbers of cells per treatment: 23, 4, 24, 11, 23, 21, 18, 10, each from at least three independent experiments. (H) Distance to the nearest centrosome in time from the indicated acute treatments. The images are maximum projection color coded by height as specified by the color bar in 1A. Statistics: unpaired t-test (n.s., non-significant, $*p < 0.05$; $**p < 0.01$; $***p < 0.001$; $****p < 0.0001$). Inh., inhibited, depl., depleted, siRNA, small interfering RNA.

CENP-E is required for polar chromosome congression only in the presence of centrioles

As polar chromosomes in the absence of CENP-E are localized close to centrosomes for prolonged duration (Fig. 1A, S1D), and as their congression capacity is positively correlated with distance from the centrosome (Fig. S1F, G), we hypothesized that centrosomes negatively impact the congression of the polar chromosome in the absence of CENP-E activity. We thus reasoned that depletion of centrioles, focal constituents of centrosomes[72], could release polar chromosome congression from its dependence on CENP-E. To deplete centrioles, we inhibited polo-like kinase 4 (Plk4) activity with centrinone, a small molecule inhibitor that blocks the centriole duplication cycle[73], and varied the duration of treatment to obtain spindle types with different numbers of centrioles on each centrosome, namely 2:2, 1:1, 1:0 and 0:0 (Fig. S5A) and combined it with CENP-E perturbations.

As a proxy of congression efficiency, we quantified the number of polar chromosomes 5 minutes after the end of spindle elongation, the duration of polar chromosomes, and the total duration of mitosis. After CENP-E perturbations, 1:1 and 2:2 spindles had, on average, about 8 polar chromosomes per spindle, whereas this number was <1 in control conditions in both spindle types (Fig. 4A, B, Video S6). In 1:0 spindles, the centriolar centrosomes (marked “1”) had about 4 polar chromosomes, similar to the equivalent centrosomes in 1:1 spindles (Fig. 4B, Video S6). Strikingly, acentriolar centrosomes (marked “0”) in 1:0 spindles rarely contained polar chromosomes, irrespectively of CENP-E activity (Fig. 4A, B, Video S6). Polar chromosomes across all spindle types persisted much longer when CENP-E was perturbed (Fig. 4C), causing extensive mitotic prolongation (Fig. S5B). Completely acentriolar 0:0 spindles, which were rarely found, had a low number of polar chromosomes in the CENP-E inhibited condition, indistinguishable from acentriolar centrosomes in 1:0 spindles (Fig. 4D, E, Video S6). These findings suggest that centrioles limit the congression of polar chromosomes if CENP-E activity is perturbed.

We did not observed difference in microtubule organization on centriolar and acentriolar centrosomes when imaging microtubules by STED microscopy, except lack of astral microtubules on acentriolar centrosomes (Fig. S5C). We also compared the dynamics of congression in 1:0 and 1:1 spindles in the CENP-E inhibited condition, and found that congression velocities were indistinguishable from each other, and from the velocity after CENP-E inhibition in 2:2 spindles (Figs. S5D-I). This suggests that the velocity of chromosome congression is robust to changes in the number of centrioles.

To check if centriole removal during prolonged mitosis would induce congression of polar chromosomes independently of Plk4 inhibition, we focused on rare cases (<10%, n=5 out of 55 cells) where spontaneous dislocation of a centriole from the centrosome in 1:1 spindles occurred in the CENP-E depleted condition (Fig. S5J)[74]. Fascinatingly, upon displacement of a centriole from the centrosome, polar chromosomes initiated congression almost instantaneously in all cases (Fig. S5J). This suggests that the presence of centrioles *per se* limits the congression of polar chromosomes in the absence of CENP-E. The inhibitory effect of centrioles on congression of polar chromosomes is independent of chromosome positioning with respect to spindle poles, as we observed that most chromosomes aligned successfully when CENP-E activity was inhibited in combination with the addition and washout of the Eg5 inhibitor, which increased the number of chromosomes behind the poles (Fig. S5K). To conclude, the presence of centrioles is required for persistence of polar chromosomes in the absence of CENP-E activity (Fig. 4F), implying that centrioles negatively impact congression of polar chromosomes.

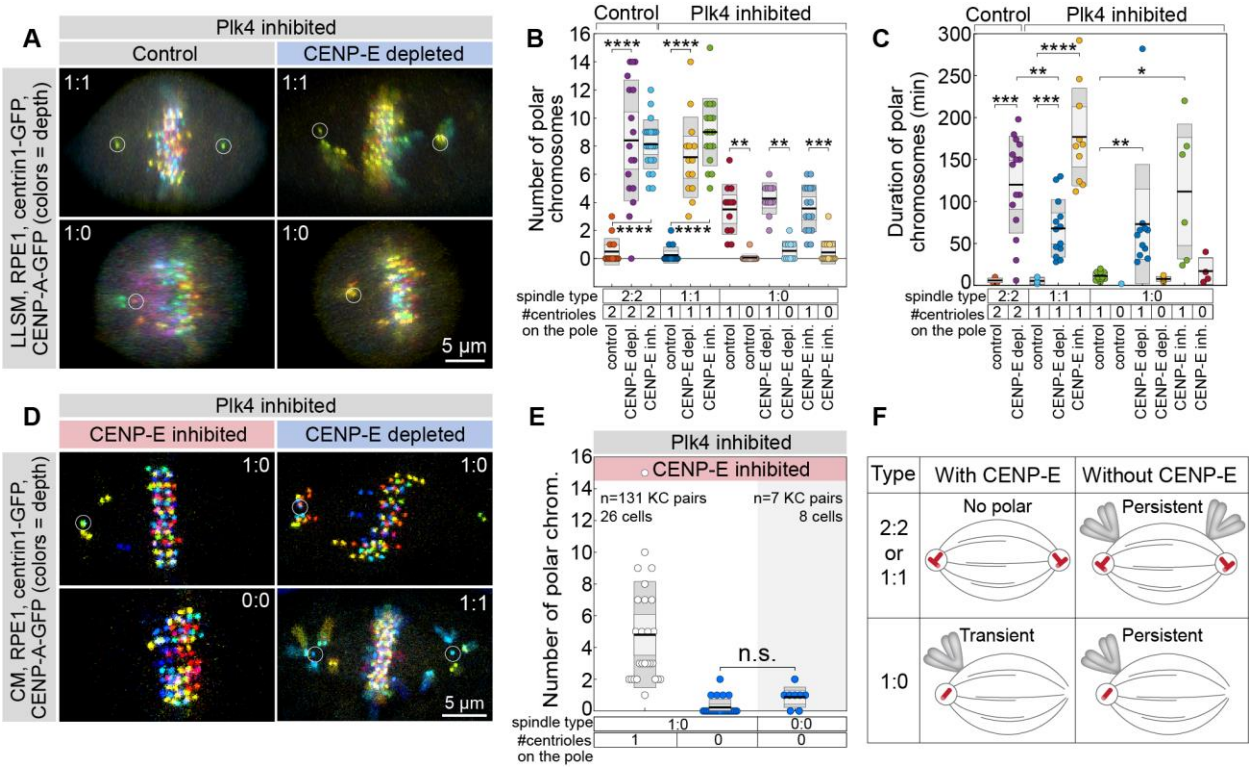

Figure 4. Centrioles limit chromosome congression in the absence of CENP-E activity. (A) Representative examples of cells expressing CENP-A-GFP and centrin1-GFP with different

numbers of centrioles (denoted by white circles) on each pole 5 minutes after spindle elongation imaged by lattice-light sheet microscopy for treatments indicated on top. (B-C) Number (B) and duration (C) of polar chromosomes after end of prometaphase spindle elongation in cells with different numbers of centrioles designated at the bottom across different indicated treatments. The black line shows the mean; the light grey and dark grey areas mark the 95% confidence interval on the mean and standard deviation, respectively. Number of cells per condition (B, C): 14, 15, 22, 16, 14, 18, 16, 16, 12, 12, 16, 16, each from at least three independent experiments. (D) Representative examples of cells expressing CENP-A-GFP and centrin1-GFP with different numbers of centrioles as indicated. (E) Number of polar chromosomes after different treatments imaged by confocal microscopy in cells with different numbers of centrioles as indicated. Experiment performed in more than three independent experiments. (F) Schemes depicting the summary of experimental results for the number and duration of polar chromosomes for cells with spindle types characterized by different numbers of centrioles with or without CENP-E activity. Images are maximum projections color coded by height as specified by the color bar in the 1A. Statistics: unpaired t-test. (n.s., non-significant, $*p < 0.05$; $**p < 0.01$; $***p < 0.001$; $****p < 0.0001$). LLSM, lattice light sheet microscopy, CM, confocal microscopy. Inh., inhbited, depl., depleted, chr., chromosomes, KC, kinetochore.

Centriolar Aurora A limits congression in the absence of CENP-E by increasing the activity of the kinetochore Aurora B and thus phosphorylation of the KMN network

To identify the molecular factors that delay chromosome congression on centriolar centrosomes in the absence of CENP-E, we checked the levels of active Aurora A on centrosomes after Plk4 inhibition under both control and CENP-E inhibited conditions. Intriguingly, we found that acentriolar centrosomes had a 4-fold lower levels of pAurA (pT288-Aurora A) compared to centriolar centrosomes, whereas the maximum difference between two centrosomes in 1:1 spindle was on average only 10% (Fig. 5A). The observed difference in pAurA between centrosomes was not CENP-E dependent (Figs. 5A, S6A), implying that CENP-E does not control the level of active Aurora A on centrosomes. This suggests that chromosomes close to centriolar centrosomes depend on CENP-E activity for congression due to a high amount of active Aurora A on such centrosomes, in contrast to acentriolar centrosomes.

We hypothesized that the difference in the level of active Aurora A on centriolar and acentriolar centrosomes would induce differential activity of kinetochore-localized Aurora B kinase on polar chromosomes, and subsequently phosphorylation of Aurora B downstream outer-kinetochore targets Hec1 and Kinetochore null protein 1 (Knl1), major components of the KMN network[75]. Indeed, the mean signal of pAurB (pT232-Aurora B) and pKnl1 (pS24, pS60-Knl1)[76] on polar kinetochores close to centriolar centrosomes was significantly higher compared to the signal on aligned kinetochores and on rare polar kinetochores at the acentriolar centrosomes under the CENP-E inhibited condition, whereas for pHec1 (pS55-Hec1)[69] a significant difference was observed only between polar and aligned kinetochores (Fig. 5B-D, S6B-D). In control cells, the level of phosphorylation was similar between aligned and rare polar kinetochores for both pAurB and pHec1, and was significantly lower compared to the same kinetochore groups in the CENP-E

inhibited condition for pAurB (Fig. S6B, C). Our results imply that in the absence of CENP-E, Aurora A on centriolar centrosomes increases the activity of outer-kinetochore Aurora B, thus increasing the phosphorylation of downstream outer-kinetochore proteins that limits the end-on binding of microtubules to the kinetochores and subsequently their congression.

If Aurora A at the centrosomes increases the activity of Aurora B, then the movement of chromosomes away from the centrosome during congression should be accompanied by a gradual decrease in aurora B-mediated phosphorylation of outer kinetochore targets. Indeed, the level of Aurora B-mediated phosphorylation of the outer kinetochore components pKnl1 and pDns1 (pS100, pS109-Dns1)[76] was inversely correlated with the distance of the chromosome from the centrosome in the absence of CENP-E activity (Fig. S6E). These findings imply that congression of polar chromosomes is accompanied by a gradual decrease in the level of Aurora B-mediated phosphorylation of the outer kinetochore components. To conclude, we show that chromosome congression is accompanied by a decrease in Aurora B activity on kinetochores resulting in a decreased phosphorylation of the KMN network components, a process essential for stable attachment of microtubules to kinetochores (Fig. 5E)[77] and chromosome congression, which is drastically accelerated by the CENP-E activity.

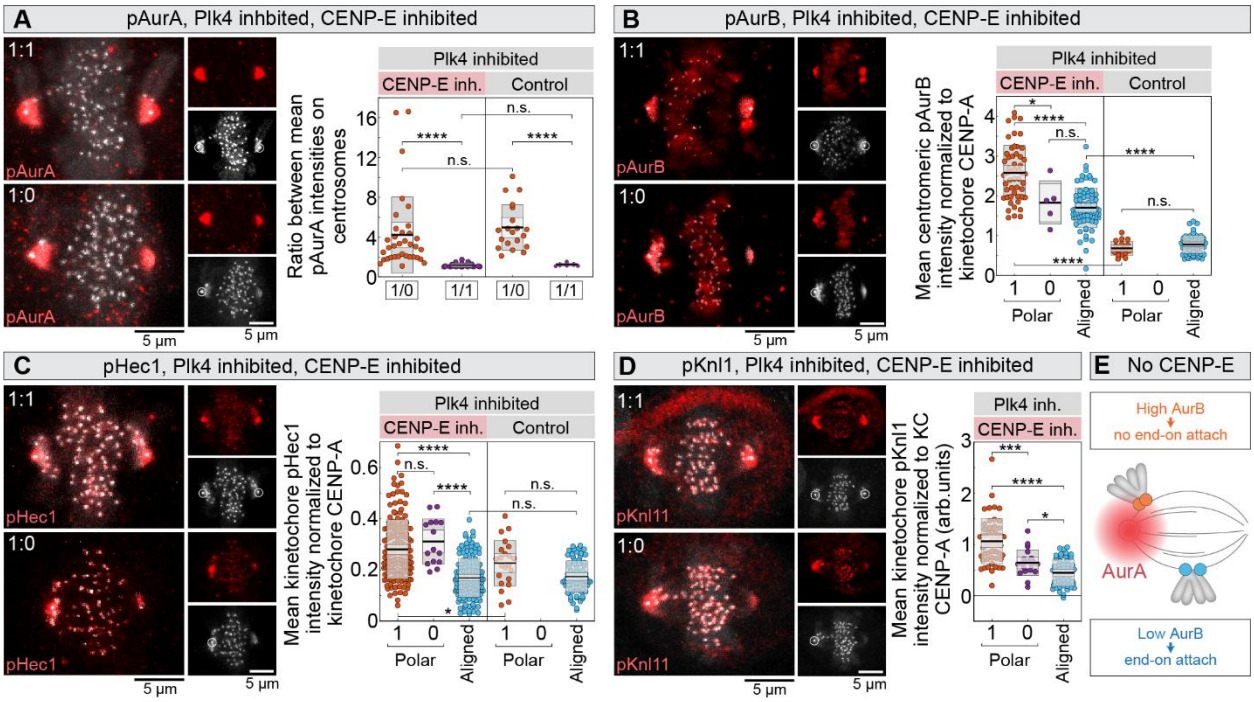

Figure 5. CENP-E negatively regulates Aurora B kinase activity and its downstream phosphorylation of kinetochore proteins close to centriolar Aurora A gradient. (A-D) Representative examples of cells expressing CENP-A-GFP and centrin1-GFP (denoted by white circles) immunostained with antibodies targeting phosphorylated residues of indicated proteins (pT288-Aurora A, pT232-Aurora B, pS55-Hec1and pS24, pS60-Knl1) with different numbers of centrioles on each pole as depicted aftertreatments indicated on top and with separated channels on right. The images are maximum projections (left). Ratio between the mean phosphorylated Aurora A in the centriolar centrosome ("1") versus the acentriolar centrosome ("0") for the

indicated treatments (A), the mean intensity of the targeted phosphorylated residues in the kinetochore as indicated and normalized to the kinetochore CENP-A intensity for the indicated kinetochore subpopulations and treatments (B-D) (right). Numbers: 35, 23, 20, 10 cells (A), 52, 5, 77 kinetochore pairs from 23 cells and 12, 33 kinetochore pairs from 19 cells (B), 153, 15, 142 kinetochore pairs from 27 cells, 22, 76 kinetochore pairs from 12 cells (C), 52, 20, 52 kinetochore pairs from 26 cells (D), all done in at least two independent experiments. (E) Scheme depicting the model based on experimental results in which Aurora A activity gradient on centriolar centrosomes upregulates Aurora B activity on kinetochore that limits the establishment of end-on attachments in the absence of CENP-E, while a low level of active Aurora B on kinetochores leads to the establishment of end-on attachments and chromosome congression independently of CENP-E. n.s., nonsignificant. Statistics: unpaired t-test (n.s., non-significant, $*p < 0.05$; $**p < 0.01$; $***p < 0.001$; $****p < 0.0001$). Inh., inhbited, depl., depleted, chr., chromosomes.

Chromosomally unstable cancer cells are highly sensitive to the absence of CENP-E in a time-dependent manner, resulting in reduced mitotic fidelity

Our results advocate that congression of polar chromosomes in non-transformed cells occurs by a lateral to end-on conversion mechanism, where CENP-E mediates essential first steps that result in a gradual reduction of phosphorylation of the outer kinetochore proteins by Aurora B kinase and subsequently chromosome biorientation. However, it remains unknown whether the described congression dynamics would hold true in cancer cell lines, which are often characterized by perturbed microtubule dynamics and deficient error correction[78–80]. To investigate how cancer cell lines respond to the absence and reactivation of CENP-E, we performed CENP-E perturbations in U-2 OS, an osteosarcoma model tumor cell line (Figs. 6A, S7A, B).

First, we observed that U-2 OS cells also displayed polar chromosomes that congressed asynchronously after CENP-E depletion (Fig. 6A, Video S7), similar to RPE-1 (Fig. 1A, Video S3) and previous reports in HeLa cells[6,32]. Interestingly, and consistently with RPE-1, chromosome movement during congression was similar between all conditions independently of CENP-E activity (Fig. 6B, C), and across all parameters of kinetochore movement (Fig. S7C-E). Likewise, the velocity of congression 4 minutes before the polar chromosome entered the plate was indistinguishable between conditions with perturbed and active CENP-E (Figs. 6D), similar to RPE-1 (Fig. 1E). However, the mean congression velocities were ~1.8 times faster in U-2 OS (Fig. 6D) than the mean velocities in the same conditions in RPE-1 (Fig. 1E). Similar to RPE-1 (Fig. S1E), congression velocities did not depend on the time elapsed from the onset of mitosis until the congression event in the CENP-E depleted condition (Fig. S7G). We conclude that the congression movement in U-2 OS cells is also CENP-E independent but is significantly faster than in RPE-1 cells.

Next, we examined how efficiently U-2 OS cells align polar chromosomes compared to RPE-1 cells in the absence of CENP-E (see Fig. S7F for depletion efficiency). We found that U-2 OS and RPE-1 cells exhibit a similar gradual decay of the number of polar chromosomes up until ~1 hour from the onset of mitosis (Figs. 6E, S7H). Although U-2 OS cells contain more

chromosomes (n=74 modal)[81] than RPE1 cells (n=46 modal)[82], RPE1 cells had a higher number of polar chromosomes 20 minutes after the onset of mitosis in the absence of CENP-E (9.86±4.72 in RPE-1, versus 7.72±4.92 in U-2 OS, Fig. S7I). This shows that U-2 OS and RPE1 cells are both sensitive to the absence of CENP-E during early mitosis. However, ∼1 hour after mitotic onset, U-2 OS cells abruptly lost the ability to initiate congression of polar chromosomes in the absence of CENP-E, since chromosome congression events were rarely observed after this point (Figs. 6E, S7H, Video S7), while RPE-1 cells continued to align polar chromosomes for hours with almost unchanged dynamics (Fig. 6E, Video S3). Therefore, U-2 OS cells are drastically more prone to chronic problems in initiating chromosome congression than RPE-1 cells in the absence of CENP-E in a time-dependent and switch-like manner.

Finally, we asked whether the large difference between the cell lines in congression capacity in the absence of CENP-E induces distinct mitotic outcomes. Indeed, we found that U-2 OS cells entered anaphase with uncongressed polar chromosomes more often than RPE-1 cells (42% versus 18%, respectively, Fig. 6F, Videos S3, S7), similar to previous reports on U-2 OS and HeLa cells[6,32]. We also observed that the severity of mitotic outcomes was time-dependent, as the cells that aligned polar chromosomes had modest delays in mitosis, which differed between the cell lines (76.68±51.98 min for U-2 OS, 143.41±66.53 min for RPE-1), compared to the larger delays observed in cells that entered anaphase in the presence of polar chromosomes, which were not different between the cell lines (291±91.76 min for U-2 OS, 303.5±94.5 min for RPE-1) (Fig. S7J). After similar mitotic delays, U-2 OS cells entered anaphase with ~13 times more polar chromosomes than RPE1 cells upon CENP-E depletion (1.56±2.61 for U-2 OS versus 0.12±0.32 for RPE-1, Fig. 6G, Video S7). We conclude that the high sensitivity of U-2 OS cells to the absence of CENP-E drastically reduces mitotic fidelity in this cancer cell line.

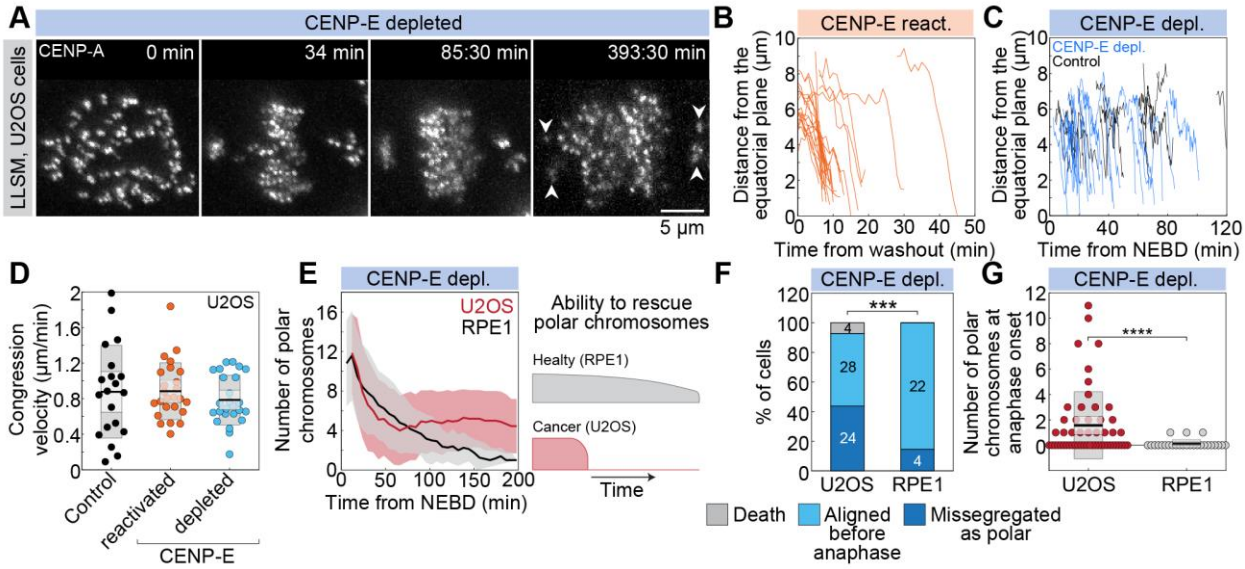

Figure 6. The congression capacity in U-2 OS cells is severely reduced in a time-dependent and switch-like manner in the absence of CENP-E. (A) Example of a representative U-2 OS cell expressing CENPA-GFP and undergoing mitosis after depletion of CENP-E. The cell was imaged using the lattice light sheet microscopy (LLSM) assay shown in 1A. The image is a maximum projection across all acquired planes. Time represents the time from the onset of mitosis. Arrowheads depict polar chromosomes in early anaphase. (B, C) Distance from the equatorial plane of kinetochore pairs in time from washout of the CENP-E inhibitor (B) or from nuclear envelope breakdown (NEBD) (C). (D) Velocity of chromosome congression during the 4-minute period that precedes complete alignment of polar chromosomes for depicted treatments. The black line shows the mean; the light grey and dark grey areas mark the 95% confidence interval on the mean and standard deviation, respectively. Numbers (B-D): control (30 cells, 64 kinetochore pairs), reactivated (10 cells, 38 kinetochore pairs), depleted (10 cells, 52 kinetochore pairs), each done in at least three independent experiments. (E) Number of polar chromosomes in time from NEBD after depletion of CENP-E in RPE-1 (gray) and U-2 OS (red) cells (left). Scheme showing the ability to rescue polar chromosomes in the absence of CENP-E as a function of time inferred from the data presented in the left part for the depicted cell lines (right). (F) Frequency of indicated chromosome mis-segregation phenotypes in anaphase across depicted cell lines. (G) Number of polar chromosomes at the onset of anaphase across the indicated cell lines. Numbers (E-G): 58 cells (U-2 OS), 26 cells (RPE-1). Statistics: unpaired t-test (n.s., non-significant, $*p < 0.05$; $**p < 0.01$; $***p < 0.001$; $****p < 0.0001$). Inh., inhibited, depl., depleted, react., reactivated, siRNA, small interfering RNA.

DISCUSSION

Here, we put forward a model of chromosome congression in which CENP-E initiates congression by opposing Aurora kinases in the vicinity of centrosomes, thereby promoting end-on microtubule attachments. This model solves the long-standing perplexity of how spatial and temporal coordination of mechanisms that regulate biorientation and chromosome congression that involve Aurora kinases and CENP-E is achieved during early mitosis[70]. Contrary to the previous models that proposed two congression mechanisms, one based on kinetochore biorientation and the other on CENP-E-driven gliding of kinetochores along spindle microtubules[1,4,19], we propose a single model of chromosome congression. The model is centered on two functional loops. First, the gradient of Aurora A kinase activity restricted to the region close to centrioles upregulates Aurora B localized on the outer kinetochore, which limits the stability of end-on attachments by phosphorylation of the components of the KMN network[45,83], and possibly also by direct phosphorylation of Hec1 by Aurora A[25] (Fig. 7A). Second, Aurora kinases phosphorylate and activate CENP-E close to centrioles[25,84], which after interaction and phosphorylation by BubR1[41], initiates transition to end-on attachments and down-regulation of Aurora B kinase activity along with phosphorylation of its downstream substrates. This event leads to the stabilization of end-on attachments on polar kinetochores, evident in the loss of Mad2, which leads to the initiation of a congression movement that presumably requires only microtubule depolymerization-driven pulling forces[13] (Fig. 7A). Bias of chromosome movement towards the metaphase plate is probably achieved by microtubule length-dependent activity of Kif18a/kinesin-8 at the plus ends of kinetochore fibers[66] and length-dependent poleward flux of sister kinetochore fibers[85]. CENP-E-mediated down-regulation of Aurora B on kinetochores is independent of phosphatases and tension[86], and probably relies on a plus tip tracking activity of CENP-E[21,41] and/or capture and sorting of microtubules by the fibrous corona and CENP-E[87]. Thus, we propose that congression operates as a negative feedback loop between the activity of Aurora kinases that oppose congression by destabilizing end-on attachments, but also activate CENP-E[25,84], which then promotes congression by opposing the activity of Aurora kinases (Fig. 7B).

The presented model provides a molecular mechanism underlying the observations that only peripheral polar chromosomes are prone to congression delays in the absence of CENP-E[4], and that most biorientation events during early mitosis occur outside the region of the spindle poles[31]. Our model also challenges the view on the role of Aurora kinases during early mitosis, as we show that Aurora kinases oppose congression near the spindle poles, which contradicts the prevailing view that kinases solely promote congression by activating CENP-E[25]. Although we showed that chromosomes can congress without CENP-E, Aurora B and protein phosphatases, Aurora kinases are essential to prohibit stabilization of erroneous syntelic end-on attachments close to the spindle pole during early prometaphase that would satisfy SAC and lead to mis-segregation of polar chromosomes[55], and phosphatases are essential for maintaining mature end-of attachments during metaphase[65]. Thus, the temporal ordering of events during early mitosis is crucial for efficient congression. From an evolutionary perspective, we propose that a minimal module for congression requires: 1) a system that forces lateral attachments close to the spindle poles, in most organisms mediated by Aurora kinases[88], 2) microtubules that make end-on

attachments, and 3) a system that down-regulates the activity of Aurora kinases, which in metazoans is mediated initially by CENP-E and later by phosphatases.

Mechanistically, CENP-E may be involved in the formation of end-on attachments by capturing the microtubules that grow from the opposite spindle half and hit the kinetochore. These microtubules could be generated at the centrosomes, along pre-existing microtubules[89], and at the fibrous corona[90,91], and all are likely to contribute to the formation of kinetochore fibers[92,93]. Furthermore, antiparallel overlaps are known to extend in human cells deep inside the spindle halves[94], especially during prometaphase[95,96], suggesting that microtubules from one spindle half are interspersed with those from the other. Moreover, C-terminal domain of CENP-E is essential for the establishment of a fibrous corona that can nucleate and sort microtubules[31,91] or serve as a hub that captures microtubules[87]. However, as we have shown that BubR1 is essential for the initiation of congression, and BubR1 recruits exclusively kinetochore-localized CENP-E[71], while corona-localized CENP-E is recruited through the RZZ complex and dynein[68], this suggests that congression initiation is mediated mostly by the kinetochore-localized CENP-E.

Related to mitosis in disease conditions, our results show that cancer U-2 OS cells are more sensitive to the absence of CENP-E than non-transformed RPE-1 cells[6], but only if mitosis prolongs for more than an hour. This has a huge impact on mitotic fidelity in the cancer cell line, as many cells enter anaphase with large numbers of polar chromosomes, leading to aneuploidy and micronucleation. We speculate that these differences arise due to divergent time-dependent changes of microtubule stability[78,97] after mitotic prolongation between chromosomally unstable cancer cells and non-transformed cells, which could preclude initiation of congression in the absence of CENP-E specifically in these cancers. Interestingly, since it was recently shown that tetraploid cells are significantly more susceptible to CENP-E inhibitors[98] and to perturbation of the Kif18a motor[99] compared to their diploid counterparts, we hypothesize that these observations could be part of a common theme of divergent responses of chromosomally stable and unstable cells to mitotic prolongation. We envisage that these divergent responses are the result of faulty chromosome congression and SAC activation in chromosomally unstable cells, which could be a valuable path to explore in the development of new tumor treatment strategies specifically targeting aneuploid cells.

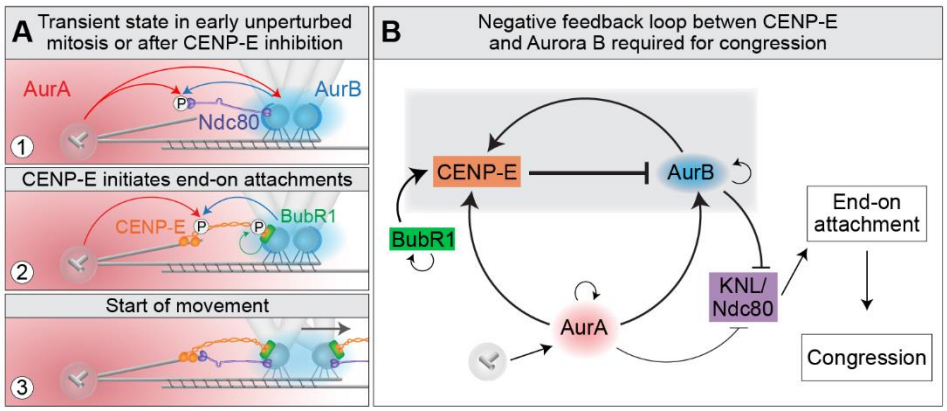

Figure 7. Model of chromosome congression that includes a functional negative feedback loop between the activity of Aurora kinases and CENP-E. (A) Polar chromosomes are initially characterized by lateral attachments of kinetochores to microtubules that fail to quickly convert to stable end-on attachments in the absence of CENP-E due to the high activity of the Aurora A gradient (AurA, red gradient centered on centrioles depicted by gray tubules) that activates outer-kinetochore Aurora B (AurB, blue crescent around kinetochores), which phosphorylate outer kinetochore proteins such as Hec1 (Ndc80) that is essential for end-on attachments of microtubules to the outer kinetochore (1). In the presence of CENP-E, and upon activation of CENP-E by Aurora kinases and BubR1 pseudokinase, CENP-E captures microtubules leading to a decrease of Aurora B-mediated phosphorylation of outer kinetochore substrates in a phosphatase-independent manner (2). This event stabilizes initial end-on attachments and leads to gradual end-on conversion, observable by gradual loss of Mad2, and subsequent movement of the polar chromosome (black arrow) towards the spindle midplane (3). (B) Functional negative feedback loop of signaling interactions involving Aurora kinases, CENP-E, and outer-kinetochore proteins Knl1/Hec1. Lines with arrows indicate activation and blunt lines indicate deactivation.

ACKNOWLEDGEMENTS

We thank Alexey Khodjakov, Helder Maiato, and Jonathon Pines for cell lines; Marin Barišić for intensive discussions and cell lines; Julie Welburn for discussions and antibodies; Magda Topić and Mia Crnogaj for help with cell culture work and preparation of inhibitors; Ivana Šarić for the drawings; and members of the Tolić, Kops, and Pavin groups for constructive comments on the manuscript. This work was funded by the European Research Council (ERC Synergy Grant, GA Number 855158), the Croatian Science Foundation (HRZZ) through Swiss-Croatian Bilateral Projects (project IPCH-2022-10-9344), and projects co-financed by the Croatian Government and the European Union through the European Regional Development Fund—the Competitiveness and Cohesion Operational Programme: IPSted (Grant KK.01.1.1.04.0057) and QuantiXLie Center of Excellence (Grant KK.01.1.1.01.0004).

AUTHOR CONTRIBUTIONS

K.V. and I.M.T conceived the project, K.V. performed all experiments, quantified, analyzed and presented the data, K.V. conceptualized and prepared original draft, K.V. and I.M.T. reviewed, edited and discussed manuscript.

MATERIALS AND METHODS

Cell lines and culture

Experiments were carried out using human hTERT-RPE1 (hTERT-immortalized retinal pigment epithelium) cells stably expressing CENP-A-GFP and human hTERT-RPE1 cells stably expressing both CENP-A-GFP and centrin1-GFP, courtesy of Alexey Khodjakov (Wadsworth Center, New York State Department of Health, Albany, NY, USA), human hTERT-RPE1 cells stably expressing CENP-A-mCerulean and Mad2-mRuby, courtesy of Jonathon Pines (Institute of Cancer Research, London, UK), and human U-2 OS (osteosarcoma patient) cells stably expressing CENP-A-GFP, courtesy of Marin Barišić (Danish Cancer Society Research Center, Copenhagen, Denmark). All cell lines were cultured in flasks in Dulbecco's Modified Eagle's Medium with 1 g/L D-glucose, pyruvate and L-glutamine (DMEM, Lonza, Basel, Switzerland), supplemented with 10% (vol/vol) heat-inactivated Fetal Bovine Serum (FBS, Sigma-Aldrich, St. Louis, MO, USA) and penicillin (100 IU/mL)/streptomycin (100 mg/mL) solution (Lonza, Basel, Switzerland). The cells were kept at 37 °C and 5% CO2 in a humidified incubator (Galaxy 170 S CO2, Eppendorf, Hamburg, Germany) and regularly passaged at the confluence of 70-80%. None of the cell lines were authenticated. All cell lines have also been regularly tested for mycoplasma contamination by examining samples for extracellular DNA staining with SiR-DNA (100 nM, Spirochrome, Stein am Rhein, Switzerland) and Hoechst 33342 dye (1 drop/2 ml of NucBlue Live ReadyProbes Reagent, Thermo Fisher Scientific, Waltham, MA, USA) and have been confirmed to be mycoplasma free.

Sample preparation and siRNAs

At 80% confluence, the DMEM medium was removed from the flask and the cells were washed with 5 ml of phosphate buffered saline (PBS). Then, 1 ml 1% trypsin/ethylenediaminetetraacetic acid (EDTA, Biochrom AG, Berlin, Germany) was added to the flask and cells were incubated at 37 °C and 5% CO2 in a humidified incubator for 5 min. After incubation, trypsin was blocked by adding 4 ml of DMEM medium. For the RNAi experiments, cells were seeded to reach 60% confluence the next day and cultured on 35 mm uncoated plates with 0.17 mm (#1.5 coverglass) glass thickness of 0.17 mm (# 1.5 coverglass) (MatTek Corporation, Ashland, MA, USA) in 1 ml of DMEM medium with the supplements described above. After one day of growth, cells were transfected with either targeting or non-targeting siRNA constructs which were diluted in OPTI-MEM medium (Life Technologies, Waltham, MA, USA) to a final concentration of 100 nM in the medium with cells. All transfections were performed 48 h before imaging using Lipofectamine RNAiMAX Reagent (Life Technologies, Waltham, MA, USA) according to the instructions provided by the manufacturer. After four hours of siRNA treatment, the medium was changed to the DMEM medium. The constructs used were: human CENP-E ON-TARGET plus SMART pool siRNA (L-003252-00-0010, Dharmacon, Lafayette, CO, USA), human PRC1 ON-TARGET plus SMART pool siRNA (L-019491-00-0020, Dharmacon), human Ndc80/Hec1 siRNA (sequence antisense: 5'- GAAUUGCAGCAGACUAUUA-3', dTdT overhangs, Sigma-Aldrich, St. Louis, MO, USA), human KIF4A siRNA (sc-60888, Santa Cruz Biotechnology), Human Kif18A siRNA (Ambion, #Cat 4390825, ID:s37882), Human Kif22/Kid siRNA (Ambion, #Cat 4392420, ID:s7911), human WAPL ON-TARGET plus SMART pool siRNA (J-026287-10-0010,

Dharmacon, Lafayette, CO, USA), human BUB1B/BuBR1 ON-TARGETplus SMART pool siRNA (L-004101-00-0005, Dharmacon, Lafayette, CO, USA), human Spindly siRNA (Sequence antisense: 5'- GAAAGGGUCUCAAACUGAA-3', dTdT overhangs, Sigma-Aldrich, St. Louis, MO, USA), and control siRNA (D-001810-10-05, Dharmacon, Lafayette, CO, USA).

Drug treatments and drug washouts

The following drugs were used: Aurora B inhibitor Barasertib (AZD1152-HQPA, Selleckchem, Munich, Germany, IC_{50} value 0.32 nM, final concentration 300 nM) added acutely before imaging, CENP-E inhibitor GSK-923295 (MedChemExpress, Monmouth Junction, NJ, USA, IC_{50} value 3.2 nM, final concentration 80 nM) added 1-4 hours before imaging in most experiments, or when noted acutely before imaging, Eg5 inhibitor Monastrol (HY-101071A/CS-6183, MedChemExpress, IC_{50} value 50 μM, final concentration 100 μM) added 3 hours before imaging or acutely before imaging, Aurora B inhibitor ZM-447439 (MedChemExpress, IC_{50} value 130 nM, final concentration 2 or 3 μM as noted) added acutely before imaging, Aurora A inhibitor MLN8054 (MedChemExpress, IC_{50} value 4 nM, final concentration 125 nM) added acutely before imaging, Bub1 inhibitor BAY-320 (MedChemExpress, IC_{50} value 680 nM, final concentration 10 μM) added acutely before imaging, Haspin inhibitor 5-Iodotubercidin (5-ITu) (MedChemExpress, IC_{50} value 5-9 nM, final concentration 2 μM) added acutely before imaging, Mps1 inhibitor AZ3146 (MedChemExpress, USA, IC_{50} value 35 nM, final concentration 500 nM) added acutely before imaging, PLK1 inhibitor BI 2536 (MedChemExpress, IC_{50} value 0.83 nM, final concentration 100 nM) added acutely before imaging, inhibitor of protein phosphatases PP1 and PP2A Okadaic acid (MedChemExpress, IC_{50} value 0.1-0.3 nM for PP2A and 15-50 nM for PP1, final concentration 1 μM) added acutely before imaging, cytoplasmic dynein inhibitor Ciliobrevin D (MedChemExpress, final concentration 20 μM) added acutely before imaging, proteasome inhibitor MG-132 (MedChemExpress, IC_{50} value 100 nM, final concentration 1 μM) added acutely before imaging, PLK4 inhibitor Centrinone (MedChemExpress, K_i value 0.16 nM, final concentration 300 nM) added 1-5 days before the imaging as noted. The stock solutions for all drugs were prepared in DMSO except okadaic acid which was prepared in ethanol. The stock solutions of all drugs were kept aliquoted at 10-50 μL at -20 °C for a maximum period of three months or at -80 °C for a maximum period of six months. For each day, new aliquots were thawed. All drugs were added to DMEM media used for cell culture to obtain the final concentration of a drug as described, except Ciliobrevin D, which was added to a serum-reduced Opti-MEM medium (Life Technologies, Waltham, MA, USA) that was placed on cells acutely before adding the drug, as Ciliobrevin D did not show any effect when used in DMEM medium with 10% FBS[62]. Drug washouts were performed by replacing drug-containing medium with 2 mL of fresh pre-warmed DMEM medium followed by four subsequent washouts with 2 mL of pre-warmed DMEM. Proteasome inhibitor MG-132 (Sigma-Aldrich) was used at a final concentration of 20 μM to arrest the cells in metaphase.

To deplete centrioles, Plk4 kinase activity was inhibited with centrinone, a small molecule inhibitor that blocks the centriole duplication cycle, and varied the duration of treatment to obtain spindles with different numbers of centrioles on each centrosome, a method established previously[73]. Subsequently, we treated Plk4-inhibited cells with CENP-E inhibitor or DMSO and

imaged cells a few hours after treatment using the same live cell imaging protocol described previously. Acute inhibition of Aurora B by ZM-447439 (3 μM) or barasertib (300 nM) induced premature anaphase onset in cells pretreated with the CENP-E inhibitor 15-30 min after the addition of Aurora B inhibitor[32]. Similarly, premature onset of anaphase was observed during the 30 min course of the imaging in cells acutely treated with the Mps1 inhibitor AZ3146 (500 nM), as expected from previous work[47]. When noted in the text, we treated CENP-E inhibited cells with the proteasome inhibitor MG-132 together with Aurora B or Mps1 inhibitors to block premature anaphase onset. MG treatment provided more time for the chromosomes to complete the alignment successfully, as in the Aurora B inhibitor alone, anaphase ensued while some chromosomes were still in the alignment process. Acute treatment of cells with dynein inhibitor 20 μM Ciliobrevin D splayed the spindle poles in all treated cells during 30 minutes after the addition of the drug, reflecting the reported role of the dynein-dynactin complex in the focus of the spindle poles in human cells[62]. Interestingly, co-inhibition of Bub1 by BAY-320 (10 μM) and Haspin by 5-ITu (2 μM) in some cells induced premature onset of anaphase during the first 20 minutes after addition of the drug, reflecting the possible role of both pathways in the maintenance of the spindle assembly checkpoint[49]. After acute treatment of CENP-E inhibited cells with the Eg5 inhibitor monastrol (50 uM), spindles quickly shortened, as expected from previous reports[100]. Similarly, acute and drastic spindle shortening was observed in most CENP-E inhibited cells after acute addition of the Aurora A inhibitor MLN8054 (125 nM), as expected from previous studies[55]. Acute inhibition of PLK1 by BI 2536 (100 nM) induced a fast block of spindle elongation and cytokinetic invasion in cells after the onset of anaphase observed only after CENP-E washout, as expected from previous reports[101]. Acute treatment of cells with Okadaic acid (1 uM) together with acute treatment with Aurora B inhibitor or CENP-E inhibitor washout produced frequent expels of aligned kinetochores from the plate and sometimes complete breakage of the integrity of metaphase plates, but only after most of the polar chromosomes had already aligned to the plate, similar to previous reports of PP1 antibody injections into HeLa cells[25].

Regarding cells imaged by confocal microscopy after the chronic inhibition of CENP-E by GSK-923295 (80 nM), all pseudo-metaphase spindles chosen for imaging were phenotypically similar between each other and between conditions where CENP-E was depleted or reactivated after washout of the CENP-E inhibitor: 1) in all cells few chromosomes were localized close to one of the spindle poles, called polar chromosomes, and their numbers ranged from 2-16 per cell; 2) occasionally in some cells few chromosomes were localized already in between spindle pole and equator; and 3) in all cells most chromosomes were already aligned and tightly packed at the metaphase plate. This type of chromosome arrangement was expected from previously published data that reported that only 10-30% of chromosomes upon NEBD require CENP-E-mediated alignment[4]. Likewise, under all conditions where CENP-E was perturbed and cells imaged by confocal microscopy during pseudo-metaphase, the overall displacement of spindle poles from each other was negligible (data not shown), consistent with cells being in a pseudo-metaphase state where there is no net change in spindle length.

Immunofluorescence

For cell labeling with phopho-Knl1, phopho-Dsn1, phosphor-Hec1, phospho-Aurora A, phospho-Aurora B, and phospho-AuroraA/B/C antibodies, RPE-1 cells expressing CENP-A-GFP and centrin1-GFP grown on glass-bottom dishes (14 mm, No. 1.5, MatTek Corporation, Darmstadt, Germany) were pre-extracted with pre-warmed PEM buffer at 37 °C (0.1 M PIPES, 0.001 M MgCl2 × 6 H2O, 0.001 M EDTA, 0.5% Triton-X-100) for 30 s at room temperature and fixed by 1 ml of pre-warmed solution of 4% paraformaldehyde (PFA) for 20 min. After fixation, cells were washed 3 times for 5 min with 1 ml of PBS and permeabilized with 0.5% Triton-X-100 solution in water for 30 min at room temperature. To block unspecific binding, cells were incubated in 1 ml of blocking buffer (2% bovine serum albumin, BSA) for 2 h at room temperature. The cells were then washed 3 times for 5 min with 1 ml of PBS and incubated with 500 µl of primary antibody solution overnight at 4°C. Antibody incubation was performed using a blocking solution composed of 0.1% Triton, 1% BSA in PBS. Following antibodies were used in this assay: rabbit monoclonal phopho-Knl1 (1.5 mg/mlgift from J. Welburn diluted 1:1000), rabbit monoclonal phopho-Dsn1 conjugated to Cy3 (0.5 mg/ml, gift from J. Welburn, diluted 1:250, diluted 1:500), rabbit monoclonal phospho-Aurora A (Thr288) (C39D8) (3079T, Cell Signalling Technology, diluted 1:500), rabbit monoclonal phospho-Aurora A (Thr288)/Aurora B (Thr232)/Aurora C (Thr198) (D12A11) (2914T, Cell Signalling Technology, diluted 1:500), rabbit polyclonal phospho-Hec1 (Ser55) (GTX70017, GeneTex, diluted 1:500), rabbit polyclonal phospho-Aurora B (Thr232) (GTX85607, GeneTex, diluted 1:500). After primary antibody, cells were washed in PBS and then incubated in 500 µL of secondary antibody solution for 45 min at room temperature. Following secondary antibodies were used in this assay: Donkey anti-rabbit IgG Alexa Fluor 647 (ab150075, Abcam, diluted 1:1000) for phopho-Dsn1, Donkey anti-rabbit IgG Alexa Fluor 594 (ab150064, Abcam, diluted 1:1000) for all others. Finally, cells were washed with 1 ml of PBS, 3 times for 10 min. Cells were imaged either immediately following the imaging or were kept at 4°C before imaging for a maximum period of one week.

To visualize alpha-tubulin in STED resolution in the RPE-1 CENP-A-GFP centrin1-GFP cell line, the ice-cold methanol protocol was avoided because it destroyed the unstable fraction of microtubules[102]. Cells were washed with cell extraction buffer (CEB) and fixed with 3.2% paraformaldehyde (PFA) and 0.1% glutaraldehyde (GA) in PEM buffer (0.1 M PIPES, 0.001 M MgCl2 × 6 H2O, 0.001 M EGTA, 0.5% Triton-X-100) for 10 min at room temperature. After fixation with PFA and GA, for quenching, cells were incubated in 1 ml of freshly prepared 0.1% borohydride in PBS for 7 min and then in 1 mL of 100 mM NH_4Cl and 100 mM glycine in PBS for 10 min at room temperature. To block nonspecific binding of antibodies, cells were incubated in 500 µL blocking/permeabilization buffer (2% normal goat serum and 0.5% Triton-X-100 in water) for 2 h at room temperature. Cells were then incubated in 500 µL of primary antibody solution containing rat anti-alpha-tubulin YL1/2 (MA1-80017, Invitrogen, CA, SAD, diluted 1:500) overnight at 4 °C. After incubation with a primary antibody, cells were washed 3 times for 10 min with 1 ml of PBS and then incubated with 500 µl of secondary antibody containing donkey anti-rat IgG Alexa Fluor 594 (ab150156, Abcam, diluted 1:300) for 2 h at room temperature, followed by wash with 1 ml of PBS 3 times for 10 min.

Imaging

Opterra I multipoint scanning confocal microscopy system (Bruker Nano Surfaces, Middleton, WI, USA) was mainly used for imaging of hTERT-RPE1 cells expressing CENP-A-GFP and Centrin1-GFP, in cells depleted of CENP-E by siRNAs and in cells with inhibited CENP-E by CENP-E inhibitor, in the assay we termed a confocal-based imaging assay. The system was mounted on a Nikon Ti-E inverted microscope equipped with a Nikon CFI Plan Apo VC 100x/1.4 numerical aperture oil objective (Nikon, Tokyo, Japan). The system was controlled with Prairie View Imaging Software (Bruker). During imaging, cells were kept at 37 ° C and at 5% CO_2 in the Okolab cage incubator (Okolab, Pozzuoli, NA, Italy). The laser power was set to 10% for the 488nm excitation laser. For optimal resolution and signal-to-noise ratio, a 60 µm pinhole aperture was used and the xy-pixel size was set to 83 nm. For excitation of GFP, a 488-nm diode laser line was used. The excitation light was separated from the emitted fluorescence using the Opterra dichroic and Barrier 488 eGFP filter set (Chroma, USA). Images were acquired with an Evolve 512 Delta Electron Multiplying Charge Coupled Device (EMCCD) camera (Photometrics, Tucson, AZ, USA) using a 150-ms exposure time and with a camera readout mode of 20 MHz. 30-60 z-stacks encompassing all focal planes with visible green signal were acquired with 0.5 µm spacing to cover the entire spindle area in depth with unidirectional xyz scan mode and with the "fast acquisition" option enabled in software. Images of six different cells were taken simultaneously every 45 s or 1 min. The total duration of the time-lapse movies was 30 min to 1 hour.

The STED confocal microscope system (Abberior Instruments) and the LSM800 laser scanning confocal system (Zeiss) were used for the remainder of the live-cell experiments we termed the confocal-based imaging assay and in hTERT-RPE1 cells expressing CENP-A-mCerulean and Mad2-mRuby after reactivation of CENP-E activity. STED microscopy was also used to image all fixed cells. STED microscopy was performed using an Expert Line easy3D STED microscope system (Abberior Instruments, Göttingen, Germany) with the 100 x/1.4NA UPLSAPO100x oil objective (Olympus, Tokio, Japan) and an avalanche photodiode detector (APD). The 488 nm line was used for excitation, with the addition of the 561 nm line for excitation and the 775 nm laser line for depletion during STED super-resolution imaging. The images were acquired using Imspector software. The xy pixel size for fixed cells was 20 nm and 10 focal planes were acquired with a 300 nm distance between the planes. For confocal live cell imaging of cells, the xy pixel size was 80 nm and 16 focal images were acquired, with 0.5 µm distance between the planes and 1 min time intervals between different frames. During imaging, live cells were kept at 37 ° C and at 5% CO_2 in the Okolab stage incubation chamber system (Okolab, Pozzuoli, NA, Italy).

LSM 800 confocal system (Zeiss) was used for the rest of live-cell confocal-based imaging in hTERT-RPE1 cells expressing CENP-A-GFP and centrin1-GFP with the following parameters: sampling in xy, 0.27 µm; z step size, 0.5 µm; total number of slices, 32; pinhole, 48.9 µm; unidirectional scan speed, 10; averaging, 2; 63x Oil DIC f/ELYRA objective (1.4 NA), 488 nm laser line (0.1% power), and detection ranges of 410–558 nm. Images were acquired using ZEN 2.6 (blue edition; Zeiss). Six cells in volumes of 15 µm were imaged sequentially every 1 minute at different positions determined right after the addition of a drug. During imaging, cells were incubated at 37 °C and 5% CO_2 using a Pecon stage incubation chamber system (Pecon, Heating Insert P S1, #130-800 005).

The Lattice Lightsheet 7 system (Zeiss) was used for live cell imaging of hTERT-RPE1 cells expressing CENP-A-GFP and Centrin1-GFP and U-2 OS cells expressing CENP-A-GFP after reactivation of CENP-E activity, in cells depleted of CENP-E by siRNAs and in cells with inhibited CENP-E by CENP-E inhibitor, in assay we called LLSM-based imaging assay. The system was equipped with an illumination objective lens 13.3×/0.4 (at a 30° angle to cover the glass) with a static phase element and a detection objective lens 44.83×/1.0 (at a 60° angle to cover the glass) with an Alvarez manipulator. The automatic immersion of water was applied from the motorized dispenser at an interval of 20 or 30 minutes. Right after sample mounting, four steps of the 'create immersion' auto immersion option were applied. The sample was illuminated with a 488-nm diode laser (power output 10 Mw) with laser power set to 1-2%. The detection module consisted of a Hamamatsu ORCA-Fusion sCMOS camera with exposure time set to 15-20 ms. The LBF 405/488/561/642 emission filter was used. During imaging, cells were kept at 37 °C and at 5% CO2 in a Zeiss stage incubation chamber system (Zeiss). The width of the imaging area in the x dimension was set from 1 to 1.5 mm.

Tracking of centrosomes and kinetochores

The spatial x and y coordinates of the kinetochore pairs were extracted in each time frame using the Low Light Tracking Tool (v.0.10), an ImageJ plugin based on the Nested Maximum Likelihood Algorithm, as previously described[100]. Tracking of polar kinetochores in the x and y planes was performed on the maximum intensity projections of all acquired z planes. Some kinetochore pairs could not be successfully tracked in all frames, mainly owing to cell and spindle movements in the z-direction over time. Spindle poles were manually tracked with points placed between the center of the two centrioles or centriole in centrinone treated cells. Kinetochore pairs that were aligned at the start of the imaging in a confocal-based imaging assay were also manually tracked in two dimensions. Quantitative analysis of all parameters was performed using custom-made MATLAB scripts (MatlabR2021a 9.10.0) scripts.

Quantification of mean Mad2, pDsn1, pKnl1, pAurora A, pAuroraB intensities of kinetochore pairs

The fluorescence intensity signal of each kinetochore in both CENP-A and respective kinetochore protein channel (Mad2, pDsn1, pKnl1) was measured by using the "*Oval selection*" tool in ImageJ with the size and position defined by the borders of the CENP-A signal of each kinetochore in the sum intensity projection of all acquired z-planes. pAurora A signal was measured using the "*Oval selection*" tool around the centriole signal as the center or around the signal of the Aurora A of the same size on the pole without centriole. The background fluorescence intensity measured in the cytoplasm was subtracted from the obtained values, and the calculated integrated intensity value was divided by the number of z-stacks used to generate the sum projection of each cell. The obtained mean intensity value subtracted for background for each kinetochore was normalized to the intensity of the CENP-A signal. For the pHec1 labeling experiments, the mean signal of Hec1 and CENP-A was measured by the same approach but on one z-plane where kinetochore CENP-A signal was the highest. The mean signal of the pAurora B was measured between extent of CENP-A signals of sister kinetochore pairs, and the mean value was normalized to mean value of CENP-A signal of each sister kinetochore pair. All movies used for the analysis were performed

using the same fixation protocol and were imaged with the same imaging parameters in at least three independent replicates.

Quantification of polar kinetochore pairs

Uncongressed polar kinetochores were defined as kinetochore pairs that are closer to one of the spindle poles than to the equatorial plane between two spindle poles. The number of polar kinetochore pairs in cells that were imaged from the onset of mitosis was quantified 12 minutes from the onset of mitosis and then every 6 minutes until the onset of anaphase or until the end of the imaging on maximum intensity projections of all acquired z planes. In cells treated with centrinone and their respective DMSO controls, the number of polar chromosomes was measured in time when the spindle finished the bipolarization process, e.g., the elongation of the spindle. This was done because all spindles of the 1:0 type with only one centriole at the beginning of mitosis went into the monopolar state and stayed in this state for variable durations before bipolarization, ranging from 10 to 50 minutes, as reported previously[103]. The duration of polar chromosomes was defined as a time from spindle bipolarization until the last polar entered the metaphase plate, or a cell entered anaphase with uncongressed polar chromosome. Duration of mitosis was defined as the time from the first signs of nuclear envelope breakdown to one frame before visible onset of anaphase defined by the separation of sister kinetochore pairs.

To calculate the distance between kinetochores in fixed samples, two points were placed at the center of the signal in each pair of kinetochores using a 'Point tool' in ImageJ. Congression velocity was calculated for each pair of kinetochores in the last 6 minutes (RPE-1) or 4 minutes (U-2 OS) before the center of the pair of kinetochores surpassed 2 µm from the equatorial plane measured as the nearest distance from a center of a pair to a plane. The angle between the kinetochore pairs and the main spindle axis was defined as an angle between a line connecting two centrosomes and a line connecting the center of the kinetochore pair and a spindle pole nearest to the respective pair.

Three types of mitotic outcomes were analyzed in CENP-E-depleted anaphase spindles in RPE-1 and U-2 OS cells: persistent polar kinetochores, repaired polar kinetochores, and death in mitosis. Cells classified as 'mis-segregated as polar' were defined as those in which kinetochores were situated outside the metaphase plate after spindle bipolarization and persisted there after the onset of anaphase. Cells classified as 'aligned before anaphase' were defined as those in which kinetochores were situated outside the metaphase plate after spindle bipolarization but aligned to the metaphase plate before anaphase onset. Cells classified as 'death' were defined as those in which kinetochores were situated outside the metaphase plate after spindle bipolarization while the cell subsequently did not enter anaphase, but instead showed signs of apoptotic blebbing and rapid disintegration of the CENP-A signal.

In images acquired using STED microscopy, lateral attachments were defined as those in which the kinetochore did not form visible attachments with microtubules that terminate at the kinetochore, defined by the CENP-A signal; end-on attachments were defined as those in which the kinetochore formed visible attachments with microtubules that terminated at the kinetochore,

defined by the CENP-A signal, with no visible microtubule signal just below or above the kinetochore.

Image processing and statistical analysis

Image processing was performed in ImageJ (National Institutes of Health, Bethesda, MD, USA). Quantification and statistical analysis were performed in MatLab. The figures were assembled in Adobe Illustrator CS6 and Adobe Photoshop CS6 (Adobe Systems, Mountain View, CA, USA). Raw images were used for quantification. The images of spindles were rotated in every frame to fit the long axis of the spindle to be parallel with the central long axis of the box in ImageJ and the spindle short axis to be parallel with the central short axis of the designated box in ImageJ. The designated box sizes were cut to the same dimensions for all panels in the figures where the same experimental setups were used across the treatments. When comparing different treatments in channels in which the same protein was labeled, the minimum and maximum intensity of that channel was set to the values in the control treatment. When indicated, the smoothing of the images was performed using the "Gaussian blur" function in ImageJ (s=0.5-1.0). Colour-coded maximum intensity projections of the z-stacks were done using the "*Temporal colour code*" tool in Fiji by applying “16-color” or “Spectrum” lookup-table (LUT) or other LUT as indicated. For the generation of univariate scatter plots, the open Matlab extension "UnivarScatter" was used (https://github.com/manulera/UnivarScatter). Data are given as mean ± standard deviation (s.t.d.), unless otherwise stated. Other dispersion measures used are defined in their respective figure captions or in Figure 1 and Figure S1 if the same measures are used across all figures. The exact values of n are given in the respective figure captions, where n represents the number of cells or the number of tracked kinetochore pairs, as defined for each n in the figure captions or tables. The number of independent experiments is also given in the figure captions. The p values were obtained using the student’s t-test of two samples (significance level was 5%), or the one-way ANOVA test (significance level was 5%), defined in figure captions. When comparing the same parameters cell by cell, we used the student’s t-test of paired two samples (significance level was 5%). $p < 0.05$ was considered statistically significant, very significant if $0.001 < p < 0.01$ and extremely significant if $p < 0.001$. Values of all significant differences are given with the degree of significance indicated ($*0.01 < p < 0.05$, $**0.001 < p < 0.01$, $***p < 0.001$, $**** < 0.0001$). For the linear regression correlation measure between two parameters, the nonparametric Spearman correlation coefficient, termed rs, was used where $p<0.001$, calculated using the 'corr' function in Matlab (Statistics Toolbox R14). No statistical methods were used to predetermine the sample size. The experiments were not randomized and, except where stated, the investigators were not blinded to allocation during experiments and outcome evaluation.

REFERENCES

1. Maiato, H., Gomes, A.M., Sousa, F., and Barisic, M. (2017). Mechanisms of Chromosome Congression during Mitosis. Biol. 2017, Vol. 6, Page 13 *6*, 13. 10.3390/BIOLOGY6010013.

2. McAinsh, A.D., and Kops, G.J.P.L. (2023). Principles and dynamics of spindle assembly checkpoint signalling. Nat. Rev. Mol. Cell Biol. *24*, 543–559. 10.1038/S41580-023-00593-Z.

3. Valdez, V.A., Neahring, L., Petry, S., and Dumont, S. (2023). Mechanisms underlying spindle assembly and robustness. Nat. Rev. Mol. Cell Biol. *24*, 523–542. 10.1038/S41580-023-00584-0.

4. Barisic, M., Aguiar, P., Geley, S., and Maiato, H. (2014). Kinetochore motors drive congression of peripheral polar chromosomes by overcoming random arm-ejection forces. Nat. Cell Biol. *16*, 1249–1256. 10.1038/NCB3060.

5. Rieder, C.L., Cole, R.W., Khodjakov, A., and Sluder, G. (1995). The checkpoint delaying anaphase in response to chromosome monoorientation is mediated by an inhibitory signal produced by unattached kinetochores. J. Cell Biol. *130*, 941–948. 10.1083/JCB.130.4.941.

6. Gomes, A.M., Orr, B., Novais-Cruz, M., De Sousa, F., Macário-Monteiro, J., Lemos, C., Ferrás, C., and Maiato, H. (2022). Micronuclei from misaligned chromosomes that satisfy the spindle assembly checkpoint in cancer cells. Curr. Biol. *32*, 4240-4254.e5. 10.1016/J.CUB.2022.08.026.

7. Tucker, J.B., Bonema, S.C., García-Varela, R., Denu, R.A., Hu, Y., McGregor, S.M., Burkard, M.E., and Weaver, B.A. (2023). Misaligned Chromosomes are a Major Source of Chromosomal Instability in Breast Cancer. Cancer Res. Commun. *3*, 54–65. 10.1158/2767-9764.CRC-22-0302.

8. Klaasen, S.J., Truong, M.A., van Jaarsveld, R.H., Koprivec, I., Štimac, V., de Vries, S.G., Risteski, P., Kodba, S., Vukušić, K., de Luca, K.L., et al. (2022). Nuclear chromosome locations dictate segregation error frequencies. Nature *607*, 604–609. 10.1038/S41586-022-04938-0.

9. Vukušić, K., and Tolić, I.M. (2022). Polar Chromosomes-Challenges of a Risky Path. Cells *11*. 10.3390/CELLS11091531.

10. Yao, X., Anderson, K.L., and Cleveland, D.W. (1997). The microtubule-dependent motor centromere-associated protein E (CENP-E) is an integral component of kinetochore corona fibers that link centromeres to spindle microtubules. J. Cell Biol. *139*, 435–447. 10.1083/JCB.139.2.435.

11. Shrestha, R.L., and Draviam, V.M. (2013). Lateral to end-on conversion of chromosome-microtubule attachment requires kinesins cenp-e and MCAK. Curr. Biol. *23*, 1514–1526. 10.1016/J.CUB.2013.06.040.

12. Bancroft, J., Auckland, P., Samora, C.P., and McAinsh, A.D. (2015). Chromosome congression is promoted by CENP-Q- and CENP-Edependent pathways. J. Cell Sci. *128*,

171–184. 10.1242/JCS.163659/-/DC1.

13. Auckland, P., and McAinsh, A.D. (2015). Building an integrated model of chromosome congression. J. Cell Sci. *128*, 3363–3374. 10.1242/JCS.169367.

14. Yen, T.J., Li, G., Schaar, B.T., Szilak, I., and Cleveland, D.W. (1992). CENP-E is a putative kinetochore motor that accumulates just before mitosis. Nature *359*, 536–539. 10.1038/359536A0.

15. Yen, T.J., Compton, D.A., Wise, D., Zinkowski, R.P., Brinkley, B.R., Earnshaw, W.C., and Cleveland, D.W. (1991). CENP-E, a novel human centromere-associated protein required for progression from metaphase to anaphase. EMBO J. *10*, 1245–1254. 10.1002/J.1460-2075.1991.TB08066.X.

16. Weaver, B.A.A., Bonday, Z.Q., Putkey, F.R., Kops, G.J.P.L., Silk, A.D., and Cleveland, D.W. (2003). Centromere-associated protein-E is essential for the mammalian mitotic checkpoint to prevent aneuploidy due to single chromosome loss. J. Cell Biol. *162*, 551–563. 10.1083/JCB.200303167.

17. Schaar, B.T., Chan, G.K.T., Maddox, P., Salmon, E.D., and Yen, T.J. (1997). CENP-E function at kinetochores is essential for chromosome alignment. J. Cell Biol. *139*, 1373–1382. 10.1083/JCB.139.6.1373.

18. Mao, Y., Desai, A., and Cleveland, D.W. (2005). Microtubule capture by CENP-E silences BubR1-dependent mitotic checkpoint signaling. J. Cell Biol. *170*, 873–880. 10.1083/JCB.200505040.

19. Kapoor, T.M., Lampson, M.A., Hergert, P., Cameron, L., Cimini, D., Salmon, E.D., McEwen, B.F., and Khodjakov, A. (2006). Chromosomes can congress to the metaphase plate before biorientation. Science (80-.). *311*, 388–391. 10.1126/SCIENCE.1122142.

20. Kim, Y., Heuser, J.E., Waterman, C.M., and Cleveland, D.W. (2008). CENP-E combines a slow, processive motor and a flexible coiled coil to produce an essential motile kinetochore tether. J. Cell Biol. *181*, 411–419. 10.1083/JCB.200802189.

21. Gudimchuk, N., Vitre, B., Kim, Y., Kiyatkin, A., Cleveland, D.W., Ataullakhanov, F.I., and Grishchuk, E.L. (2013). Kinetochore kinesin CENP-E is a processive bi-directional tracker of dynamic microtubule tips. Nat. Cell Biol. *15*, 1079–1088. 10.1038/NCB2831.

22. Kapoor, T.M., Mayer, T.U., Coughlin, M.L., and Mitchison, T.J. (2000). Probing spindle assembly mechanisms with monastrol, a small molecule inhibitor of the mitotic kinesin, Eg5. J. Cell Biol. *150*, 975–988. 10.1083/JCB.150.5.975.

23. Cai, S., O'Connell, C.B., Khodjakov, A., and Walczak, C.E. (2009). Chromosome congression in the absence of kinetochore fibres. Nat. Cell Biol. *11*, 832–838. 10.1038/NCB1890.

24. Walczak, C.E., Cai, S., and Khodjakov, A. (2010). Mechanisms of chromosome behaviour during mitosis. Nat. Rev. Mol. Cell Biol. *11*, 91–102. 10.1038/NRM2832.

25. Kim, Y., Holland, A.J., Lan, W., and Cleveland, D.W. (2010). Aurora kinases and protein phosphatase 1 mediate chromosome congression through regulation of CENP-E. Cell *142*,

444–455. 10.1016/J.CELL.2010.06.039.

26. Barisic, M., Silva E Sousa, R., Tripathy, S.K., Magiera, M.M., Zaytsev, A. V., Pereira, A.L., Janke, C., Grishchuk, E.L., and Maiato, H. (2015). Microtubule detyrosination guides chromosomes during mitosis. Science (80-.). *348*, 799–803. 10.1126/SCIENCE.AAA5175.

27. Barisic, M., and Maiato, H. (2015). Dynein prevents erroneous kinetochore-microtubule attachments in mitosis. Cell Cycle *14*, 3356. 10.1080/15384101.2015.1089369.

28. Kops, G.J.P.L., and Gassmann, R. (2020). Crowning the Kinetochore: The Fibrous Corona in Chromosome Segregation. Trends Cell Biol. *30*, 653–667. 10.1016/J.TCB.2020.04.006.

29. Matković, J., Ghosh, S., Ćosić, M., Eibes, S., Barišić, M., Pavin, N., and Tolić, I.M. (2022). Kinetochore- and chromosome-driven transition of microtubules into bundles promotes spindle assembly. Nat. Commun. *13*. 10.1038/S41467-022-34957-4.

30. Chakraborty, M., Tarasovetc, E. V., Zaytsev, A. V., Godzi, M., Figueiredo, A.C., Ataullakhanov, F.I., and Grishchuk, E.L. (2019). Microtubule end conversion mediated by motors and diffusing proteins with no intrinsic microtubule end-binding activity. Nat. Commun. *10*. 10.1038/S41467-019-09411-7.

31. Renda, F., Miles, C., Tikhonenko, I., Fisher, R., Carlini, L., Kapoor, T.M., Mogilner, A., and Khodjakov, A. (2022). Non-centrosomal microtubules at kinetochores promote rapid chromosome biorientation during mitosis in human cells. Curr. Biol. 10.1016/J.CUB.2022.01.013.

32. Maia, A.F., Feijão, T., Vromans, M.J.M., Sunkel, C.E., and Lens, S.M.A. (2010). Aurora B kinase cooperates with CENP-E to promote timely anaphase onset. Chromosoma *119*, 405–413. 10.1007/S00412-010-0265-X/FIGURES/8.

33. Iemura, K., and Tanaka, K. (2015). Chromokinesin Kid and kinetochore kinesin CENP-E differentially support chromosome congression without end-on attachment to microtubules. Nat. Commun. *6*. 10.1038/NCOMMS7447.

34. McEwen, B.F., Heagle, A.B., Cassels, G.O., Buttle, K.F., and Rieder, C.L. (1997). Kinetochore fiber maturation in PtK1 cells and its implications for the mechanisms of chromosome congression and anaphase onset. J. Cell Biol. *137*, 1567–1580. 10.1083/jcb.137.7.1567.

35. Magidson, V., O'Connell, C.B., Lončarek, J., Paul, R., Mogilner, A., and Khodjakov, A. (2011). The spatial arrangement of chromosomes during prometaphase facilitates spindle assembly. Cell *146*, 555–567. 10.1016/J.CELL.2011.07.012.

36. Wood, K.W., Lad, L., Luo, L., Qian, X., Knight, S.D., Nevins, N., Brejc, K., Sutton, D., Gilmartin, A.G., Chua, P.R., et al. (2010). Antitumor activity of an allosteric inhibitor of centromere-associated protein-E. Proc. Natl. Acad. Sci. U. S. A. *107*, 5839–5844. 10.1073/PNAS.0915068107.

37. Tovini, L., and McClelland, S.E. (2019). Impaired CENP-E Function Renders Large Chromosomes More Vulnerable to Congression Failure. Biomol. 2019, Vol. 9, Page 44 *9*, 44. 10.3390/BIOM9020044.

38. Drpic, D., Pereira, A.J., Barisic, M., Maresca, T.J., and Maiato, H. (2015). Polar Ejection Forces Promote the Conversion from Lateral to End-on Kinetochore-Microtubule Attachments on Mono-oriented Chromosomes. Cell Rep. *13*, 460–468. 10.1016/J.CELREP.2015.08.008.

39. Magidson, V., Paul, R., Yang, N., Ault, J.G., O'Connell, C.B., Tikhonenko, I., Mcewen, B.F., Mogilner, A., and Khodjakov, A. (2015). Adaptive changes in the kinetochore architecture facilitate proper spindle assembly. Nat. Cell Biol. *17*, 1134–1144. 10.1038/NCB3223.

40. Itoh, G., Ikeda, M., Iemura, K., Amin, M.A., Kuriyama, S., Tanaka, M., Mizuno, N., Osakada, H., Haraguchi, T., and Tanaka, K. (2018). Lateral attachment of kinetochores to microtubules is enriched in prometaphase rosette and facilitates chromosome alignment and bi-orientation establishment. Sci. Rep. *8*. 10.1038/S41598-018-22164-5.

41. Huang, Y., Lin, L., Liu, X., Ye, S., Yao, P.Y., Wang, W., Yang, F., Gao, X., Li, J., Zhang, Y., et al. (2019). BubR1 phosphorylates CENP-E as a switch enabling the transition from lateral association to end-on capture of spindle microtubules. Cell Res. *29*, 562. 10.1038/S41422-019-0178-Z.

42. Chen, R.H., Waters, J.C., Salmon, E.D., and Murray, A.W. (1996). Association of spindle assembly checkpoint component XMAD2 with unattached kinetochores. Science (80-.). *274*, 242–246. 10.1126/SCIENCE.274.5285.242.

43. Collin, P., Nashchekina, O., Walker, R., and Pines, J. (2013). The spindle assembly checkpoint works like a rheostat rather than a toggle switch. Nat. Cell Biol. *15*, 1378–1385. 10.1038/ncb2855.

44. Kuhn, J., and Dumont, S. (2017). Spindle assembly checkpoint satisfaction occurs via end-on but not lateral attachments under tension. J. Cell Biol. *216*, 1533–1542. 10.1083/JCB.201611104.

45. Shrestha, R.L., Conti, D., Tamura, N., Braun, D., Ramalingam, R.A., Cieslinski, K., Ries, J., and Draviam, V.M. (2017). Aurora-B kinase pathway controls the lateral to end-on conversion of kinetochore-microtubule attachments in human cells. Nat. Commun. *8*. 10.1038/S41467-017-00209-Z.

46. Ditchfield, C., Johnson, V.L., Tighe, A., Ellston, R., Haworth, C., Johnson, T., Mortlock, A., Keen, N., and Taylor, S.S. (2003). Aurora B couples chromosome alignment with anaphase by targeting BubR1, Mad2, and Cenp-E to kinetochores. J. Cell Biol. *161*, 267–280. 10.1083/JCB.200208091.

47. Santaguida, S., Vernieri, C., Villa, F., Ciliberto, A., and Musacchio, A. (2011). Evidence that Aurora B is implicated in spindle checkpoint signalling independently of error correction. EMBO J. *30*, 1508–1519. 10.1038/EMBOJ.2011.70.

48. Yang, J., Ikezoe, T., Nishioka, C., Tasaka, T., Taniguchi, A., Kuwayama, Y., Komatsu, N., Bandobashi, K., Togitani, K., Koeffler, H.P., et al. (2007). AZD1152, a novel and selective aurora B kinase inhibitor, induces growth arrest, apoptosis, and sensitization for tubulin depolymerizing agent or topoisomerase II inhibitor in human acute leukemia cells in vitro and in vivo. Blood *110*, 2034–2040. 10.1182/BLOOD-2007-02-073700.

49. Hengeveld, R.C.C., Vromans, M.J.M., Vleugel, M., Hadders, M.A., and Lens, S.M.A. (2017). Inner centromere localization of the CPC maintains centromere cohesion and allows mitotic checkpoint silencing. Nat. Commun. *8*. 10.1038/ncomms15542.

50. Su, K.C., Barry, Z., Schweizer, N., Maiato, H., Bathe, M., and Cheeseman, I.M.P. (2016). A Regulatory Switch Alters Chromosome Motions at the Metaphase-to-Anaphase Transition. Cell Rep. *17*, 1728–1738. 10.1016/J.CELREP.2016.10.046.

51. Hindriksen, S., Lens, S.M.A., and Hadders, M.A. (2017). The ins and outs of Aurora B inner centromere localization. Front. Cell Dev. Biol. *5*, 112. 10.3389/FCELL.2017.00112/BIBTEX.

52. Cane, S., Ye, A.A., Luks-Morgan, S.J., and Maresca, T.J. (2013). Elevated polar ejection forces stabilize kinetochore-microtubule attachments. J. Cell Biol. *200*, 203–218. 10.1083/JCB.201211119.

53. Ehlén, Å., Martin, C., Miron, S., Julien, M., Theillet, F.X., Ropars, V., Sessa, G., Beaurepere, R., Boucherit, V., Duchambon, P., et al. (2020). Proper chromosome alignment depends on BRCA2 phosphorylation by PLK1. Nat. Commun. 2020 111 *11*, 1–21. 10.1038/s41467-020-15689-9.

54. Ali, A., and Stukenberg, P.T. (2023). Aurora kinases: Generators of spatial control during mitosis. Front. Cell Dev. Biol. *11*, 265. 10.3389/FCELL.2023.1139367/BIBTEX.

55. Ye, A.A., Deretic, J., Hoel, C.M., Hinman, A.W., Cimini, D., Welburn, J.P., and Maresca, T.J. (2015). Aurora A Kinase Contributes to a Pole-Based Error Correction Pathway. Curr. Biol. *25*, 1842–1851. 10.1016/J.CUB.2015.06.021.

56. Dai, J., Sultan, S., Taylor, S.S., and Higgins, J.M.G. (2005). The kinase haspin is required for mitotic histone H3 Thr 3 phosphorylation and normal metaphase chromosome alignment. Genes Dev. *19*, 472–488. 10.1101/GAD.1267105.

57. Kawashima, S.A., Tsukahara, T., Langegger, M., Hauf, S., Kitajima, T.S., and Watanabe, Y. (2007). Shugoshin enables tension-generating attachment of kinetochores by loading Aurora to centromeres. Genes Dev. *21*, 420–435. 10.1101/GAD.1497307.

58. Broad, A.J., DeLuca, K.F., and DeLuca, J.G. (2020). Aurora B kinase is recruited to multiple discrete kinetochore and centromere regions in human cells. J. Cell Biol. *219*. 10.1083/JCB.201905144.

59. Hadders, M.A., Hindriksen, S., Truong, M.A., Mhaskar, A.N., Pepijn Wopken, J., Vromans, M.J.M., and Lens, S.M.A. (2020). Untangling the contribution of Haspin and Bub1 to Aurora B function during mitosis. J. Cell Biol. *219*. 10.1083/JCB.201907087.

60. Barisic, M., Sohm, B., Mikolcevic, P., Wandke, C., Rauch, V., Ringer, T., Hess, M., Bonn, G., and Geley, S. (2010). Spindly/CCDC99 is required for efficient chromosome congression and mitotic checkpoint regulation. Mol. Biol. Cell *21*, 1968–1981. 10.1091/MBC.E09-04-0356/ASSET/IMAGES/LARGE/ZMK0121094770007.JPEG.

61. Gassmann, R., Holland, A.J., Varma, D., Wan, X., Çivril, F., Cleveland, D.W., Oegema, K., Salmon, E.D., and Desai, A. (2010). Removal of Spindly from microtubule-attached kinetochores controls spindle checkpoint silencing in human cells. Genes Dev. *24*, 957–

971. 10.1101/GAD.1886810.

62. Firestone, A.J., Weinger, J.S., Maldonado, M., Barlan, K., Langston, L.D., O'Donnell, M., Gelfand, V.I., Kapoor, T.M., and Chen, J.K. (2012). Small-molecule inhibitors of the AAA+ ATPase motor cytoplasmic dynein. Nature *484*, 125–129. 10.1038/NATURE10936.

63. Kajtez, J., Solomatina, A., Novak, M., Polak, B., Vukušić, K., Rüdiger, J., Cojoc, G., Milas, A., Šumanovac Šestak, I., Risteski, P., et al. (2016). Overlap microtubules link sister k-fibres and balance the forces on bi-oriented kinetochores. Nat. Commun. *7*. 10.1038/NCOMMS10298.

64. Polak, B., Risteski, P., Lesjak, S., and Tolić, I.M. (2017). PRC 1-labeled microtubule bundles and kinetochore pairs show one-to-one association in metaphase . EMBO Rep. *18*, 217–230. 10.15252/EMBR.201642650.

65. Song, X., Conti, D., Shrestha, R.L., Braun, D., and Draviam, V.M. (2021). Counteraction between Astrin-PP1 and Cyclin-B-CDK1 pathways protects chromosome-microtubule attachments independent of biorientation. Nat. Commun. *12*. 10.1038/S41467-021-27131-9.

66. Stumpff, J., von Dassow, G., Wagenbach, M., Asbury, C., and Wordeman, L. (2008). The Kinesin-8 Motor Kif18A Suppresses Kinetochore Movements to Control Mitotic Chromosome Alignment. Dev. Cell *14*, 252–262. 10.1016/J.DEVCEL.2007.11.014.

67. Lampson, M.A., Renduchitala, K., Khodjakov, A., and Kapoor, T.M. (2004). Correcting improper chromosome-spindle attachments during cell division. Nat. Cell Biol. *6*, 232–237. 10.1038/ncb1102.

68. Cmentowski, V., Ciossani, G., d'Amico, E., Wohlgemuth, S., Owa, M., Dynlacht, B., and Musacchio, A. (2023). A mechanism that integrates microtubule motors of opposite polarity at the kinetochore corona. bioRxiv, 2023.04.25.538277. 10.1101/2023.04.25.538277.

69. DeLuca, J.G., Gall, W.E., Ciferri, C., Cimini, D., Musacchio, A., and Salmon, E.D. (2006). Kinetochore Microtubule Dynamics and Attachment Stability Are Regulated by Hec1. Cell *127*, 969–982. 10.1016/J.CELL.2006.09.047.

70. Lampson, M.A., and Kapoor, T.M. (2005). The human mitotic checkpoint protein BubR1 regulates chromosome-spindle attachments. Nat. Cell Biol. *7*, 93–98. 10.1038/NCB1208.

71. Legal, T., Hayward, D., Gluszek-Kustusz, A., Blackburn, E.A., Spanos, C., Rappsilber, J., Gruneberg, U., and Welburn, J.P.I. (2020). The C-terminal helix of BubR1 is essential for CENP-E-dependent chromosome alignment. J. Cell Sci. *133*. 10.1242/JCS.246025.

72. Vasquez-Limeta, A., and Loncarek, J. (2021). Human centrosome organization and function in interphase and mitosis. Semin. Cell Dev. Biol. *117*, 30–41. 10.1016/j.semcdb.2021.03.020.

73. Wong, Y.L., Anzola, J. V., Davis, R.L., Yoon, M., Motamedi, A., Kroll, A., Seo, C.P., Hsia, J.E., Kim, S.K., Mitchell, J.W., et al. (2015). Reversible centriole depletion with an inhibitor of Polo-like kinase 4. Science *348*, 1155. 10.1126/SCIENCE.AAA5111.

74. McEwen, B.F., Chan, G.K.T., Zubrowski, B., Savoian, M.S., Sauer, M.T., and Yen, T.J. (2001). CENP-E is essential for reliable bioriented spindle attachment, but chromosome alignment can be achieved via redundant mechanisms in mammalian cells. Mol. Biol. Cell *12*, 2776–2789. 10.1091/MBC.12.9.2776.

75. Navarro, A.P., and Cheeseman, I.M. (2021). Kinetochore assembly throughout the cell cycle. Semin. Cell Dev. Biol. *117*, 62–74. 10.1016/J.SEMCDB.2021.03.008.

76. Welburn, J.P.I., Vleugel, M., Liu, D., Yates, J.R., Lampson, M.A., Fukagawa, T., and Cheeseman, I.M. (2010). Aurora B Phosphorylates Spatially Distinct Targets to Differentially Regulate the Kinetochore-Microtubule Interface. Mol. Cell *38*, 383–392. 10.1016/J.MOLCEL.2010.02.034.

77. Cheeseman, I.M., Chappie, J.S., Wilson-Kubalek, E.M., and Desai, A. (2006). The Conserved KMN Network Constitutes the Core Microtubule-Binding Site of the Kinetochore. Cell *127*, 983–997. 10.1016/J.CELL.2006.09.039.

78. Bakhoum, S.F., Genovese, G., and Compton, D.A. (2009). Deviant kinetochore microtubule dynamics underlie chromosomal instability. Curr. Biol. *19*, 1937–1942. 10.1016/J.CUB.2009.09.055.

79. Salimian, K.J., Ballister, E.R., Smoak, E.M., Wood, S., Panchenko, T., Lampson, M.A., and Black, B.E. (2011). Feedback control in sensing chromosome biorientation by the Aurora B kinase. Curr. Biol. *21*, 1158–1165. 10.1016/J.CUB.2011.06.015.

80. Ertych, N., Stolz, A., Stenzinger, A., Weichert, W., Kaulfuß, S., Burfeind, P., Aigner, A., Wordeman, L., and Bastians, H. (2014). Increased microtubule assembly rates influence chromosomal instability in colorectal cancer cells. Nat. Cell Biol. *16*, 779–791. 10.1038/NCB2994.

81. Zeng, J., Hills, S.A., Ozono, E., and Diffley, J.F.X. (2023). Cyclin E-induced replicative stress drives p53-dependent whole-genome duplication. Cell *186*, 528-542.e14. 10.1016/J.CELL.2022.12.036.

82. Jiang, X.R., Jimenez, G., Chang, E., Frolkis, M., Kusler, B., Sage, M., Beeche, M., Bodnar, A.G., Wahl, G.M., Tlsty, T.D., et al. (1999). Telomerase expression in human somatic cells does not induce changes associated with a transformed phenotype. Nat. Genet. *21*, 111–1114. 10.1038/5056.

83. DeLuca, K.F., Lens, S.M.A., and DeLuca, J.G. (2011). Temporal changes in Hec1 phosphorylation control kinetochore–microtubule attachment stability during mitosis. J. Cell Sci. *124*, 622–634. 10.1242/JCS.072629.

84. Eibes, S., Rajendraprasad, G., Guasch-Boldu, C., Kubat, M., Steblyanko, Y., and Barisic, M. (2023). CENP-E activation by Aurora A and B controls kinetochore fibrous corona disassembly. Nat. Commun. 2023 141 *14*, 1–14. 10.1038/s41467-023-41091-2.

85. Risteski, P., Božan, D., Jagrić, M., Bosilj, A., Pavin, N., and Tolić, I.M. (2022). Length-dependent poleward flux of sister kinetochore fibers promotes chromosome alignment. Cell Rep. *40*. 10.1016/J.CELREP.2022.111169.

86. Taveras, C., Liu, C., and Mao, Y. (2019). A tension-independent mechanism reduces

Aurora B-mediated phosphorylation upon microtubule capture by CENP-E at the kinetochore. Cell Cycle *18*, 1349. 10.1080/15384101.2019.1617615.

87. Sacristan, C., Ahmad, M.U.D., Keller, J., Fermie, J., Groenewold, V., Tromer, E., Fish, A., Melero, R., Carazo, J.M., Klumperman, J., et al. (2018). Dynamic kinetochore size regulation promotes microtubule capture and chromosome biorientation in mitosis. Nat. Cell Biol. 2018 207 *20*, 800–810. 10.1038/s41556-018-0130-3.

88. Carmena, M., Ruchaud, S., and Earnshaw, W.C. (2009). Making the Auroras glow: regulation of Aurora A and B kinase function by interacting proteins. Curr. Opin. Cell Biol. *21*, 796. 10.1016/J.CEB.2009.09.008.

89. Uehara, R., Nozawa, R.S., Tomioka, A., Petry, S., Vale, R.D., Obuse, C., and Goshima, G. (2009). The augmin complex plays a critical role in spindle microtubule generation for mitotic progression and cytokinesis in human cells. Proc. Natl. Acad. Sci. U. S. A. *106*, 6998–7003. 10.1073/PNAS.0901587106.

90. Sikirzhytski, V., Renda, F., Tikhonenko, I., Magidson, V., McEwen, B.F., and Khodjakov, A. (2018). Microtubules assemble near most kinetochores during early prometaphase in human cells. J. Cell Biol. *217*, 2647–2659. 10.1083/JCB.201710094/VIDEO-8.

91. Wu, J., Larreategui-Aparicio, A., Lambers, M.L.A., Bodor, D.L., Klaasen, S.J., Tollenaar, E., de Ruijter-Villani, M., and Kops, G.J.P.L. (2023). Microtubule nucleation from the fibrous corona by LIC1-pericentrin promotes chromosome congression. Curr. Biol. *33*. 10.1016/J.CUB.2023.01.010.

92. Štimac, V., Koprivec, I., Manenica, M., Simunić, J., and Tolić, I.M. (2022). Augmin prevents merotelic attachments by promoting proper arrangement of bridging and kinetochore fibers. Elife *11*. 10.7554/ELIFE.83287.

93. Almeida, A.C., Soares-De-Oliveira, J., Drpic, D., Aguiar, P., Nio, A., Pereira, J., Maiato, H., Cheeseman, L.P., Damas, J., Lewin, H.A., et al. (2022). Augmin-dependent microtubule self-organization drives kinetochore fiber maturation in mammals. Cell Rep. *39*, 110610. 10.1016/J.CELREP.2022.110610.

94. Kiewisz, R., Fabig, G., Conway, W., Baum, D., Needleman, D., and Müller-Reichert, T. (2022). Three-dimensional structure of kinetochore-fibers in human mitotic spindles. Elife *11*. 10.7554/ELIFE.75459.

95. Steblyanko, Y., Rajendraprasad, G., Osswald, M., Eibes, S., Jacome, A., Geley, S., Pereira, A.J., Maiato, H., and Barisic, M. (2020). Microtubule poleward flux in human cells is driven by the coordinated action of four kinesins. EMBO J. *39*, e105432. 10.15252/EMBJ.2020105432.

96. Betzig, E., Yamashita, N., Morita, M., Legant, W.R., Chen, B.-C., Yokota, H., and Mimori-Kiyosue, Y. (2015). Three-dimensional tracking of plus-tips by lattice light-sheet microscopy permits the quantification of microtubule growth trajectories within the mitotic apparatus. J. Biomed. Opt. *20*, 1. 10.1117/1.JBO.20.10.101206.

97. Kabeche, L., and Compton, D.A. (2013). Cyclin A regulates kinetochore microtubules to promote faithful chromosome segregation. Nature *502*, 110–113.

10.1038/NATURE12507.

98. Yoshizawa, K., Matsura, A., Shimada, M., Ishida-Ishihara, S., Sato, F., Yamamoto, T., Yaguchi, K., Kawamoto, E., Kuroda, T., Matsuo, K., et al. (2023). Tetraploidy-linked sensitization to CENP-E inhibition in human cells. Mol. Oncol. *17*, 1148–1166. 10.1002/1878-0261.13379.

99. Quinton, R.J., DiDomizio, A., Vittoria, M.A., Kotýnková, K., Ticas, C.J., Patel, S., Koga, Y., Vakhshoorzadeh, J., Hermance, N., Kuroda, T.S., et al. (2021). Whole-genome doubling confers unique genetic vulnerabilities on tumour cells. Nature *590*, 492–497. 10.1038/S41586-020-03133-3.

100. Vukušić, K., Ponjavić, I., Buđa, R., Risteski, P., and Tolić, I.M. (2021). Microtubule-sliding modules based on kinesins EG5 and PRC1-dependent KIF4A drive human spindle elongation. Dev. Cell *56*, 1253-1267.e10. 10.1016/J.DEVCEL.2021.04.005/ATTACHMENT/680C448C-DA20-433C-9F27-C90D96D86C9D/MMC1.PDF.

101. Petronczki, M., Glotzer, M., Kraut, N., and Peters, J.M. (2007). Polo-like kinase 1 triggers the initiation of cytokinesis in human cells by promoting recruitment of the RhoGEF Ect2 to the central spindle. Dev. Cell *12*, 713–725. 10.1016/J.DEVCEL.2007.03.013.

102. Ponjavić, I., Vukušić, K., and Tolić, I.M. (2021). Expansion microscopy of the mitotic spindle. Methods Cell Biol. *161*, 247–274. 10.1016/BS.MCB.2020.04.014.

103. Dudka, D., Castrogiovanni, C., Liaudet, N., Vassal, H., and Meraldi, P. (2019). Spindle-Length-Dependent HURP Localization Allows Centrosomes to Control Kinetochore-Fiber Plus-End Dynamics. Curr. Biol. *29*, 3563-3578.e6. 10.1016/J.CUB.2019.08.061.

SUPPLEMENTAL INFORMATION

CENP-E initiates chromosome congression by opposing Aurora kinases to promote end-on microtubule attachments close to centrosomes

Kruno Vukušić, Iva M. Tolić

Supplementary Figure 1

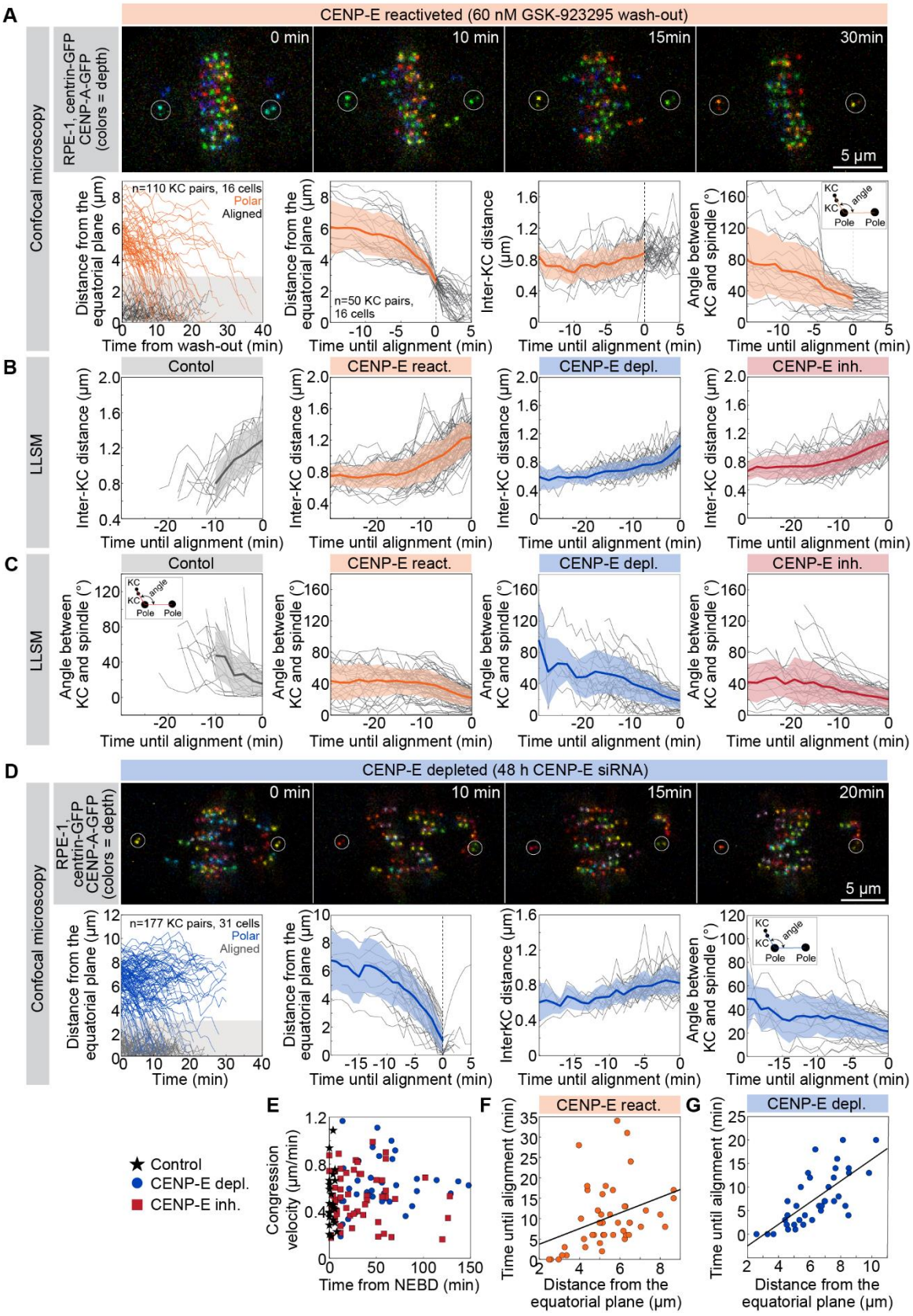

Figure S1. Various parameters of chromosome movement during congression are similar in cells with and without CENP-E activity, related to Figure 1. (A) Representative example of RPE1 cell expressing CENP-A-GFP and centrin1-GFP in different frames as depicted after wash-out of the CENP-E inhibitor 80 nM GSK923295 and imaging by confocal microscopy. The image is a maximum projection color coded by depth as specified by the color bar on figure 1A (top). Distance from the equatorial plane of sister kinetochores for initially polar (orange lines) and aligned (black lines) pairs in time from the washout of the CENP-E inhibitor, distance from the equatorial plane of sister kinetochores for initially polar kinetochore pairs, distance between sister kinetochores (inter-KC), and angle between sister kinetochores and main spindle axis, as depicted on a scheme in top-left graph in time until alignment of kinetochore pair across indicated treatment. Thick lines represent means, and grey areas over means represent standard deviations (bottom). Centrioles are rounded by the white circle. (B) Distance between sister kinetochores (inter-KC) in time until alignment of kinetochore pair across indicated treatments for cells imaged by lettice light sheet microscopy (LLSM). (C) angle between sister kinetochores and main spindle axis, as depicted on a scheme in top-left graph in time until alignment of kinetochore pair across indicated treatments for cells imaged by lettice light sheet microscopy (LLSM). (D) Representative example of RPE1 cell expressing CENP-A-GFP and centrin1-GFP in different frames as depicted after depletion of CENP-E for 48h and imaged by confocal microscopy. The image is a maximum projection color coded by depth as specified by the color bar on figure 1A (top). Distance from the equatorial plane of sister kinetochores for initially polar (blue lines) and aligned (black lines) pairs in time from the washout of the CENP-E inhibitor, distance from the equatorial plane of sister kinetochores for initialy polar kinetochore pairs, distance between sister kinetochores (inter-KC), and angle between sister kinetochores and main spindle axis, as depicted on a scheme in top-left graph in time until alignment of kinetochore pair across indicated treatment. Thick lines represent means, and grey areas over means represent standard deviations (bottom). E) Congression velocity for polar kinetochore pairs during last 6 minutes of chromosome congression versus time from the nuclear envelope breakdown (NEBD) for treatments indicated in legend on left. (F and G) Distance to the equatorial plane of the sister kinetochore pairs versus the time of alignment of each pair in the cells after washing out of the CENP-E inhibitor (F) and the depletion of CENP-E (G), where line represents regression. KC, kinetochore, depl., depletion, inh., inhibition, react., reactivation, NEBD, nuclear envelope breakdown.

Supplementary Figure 2

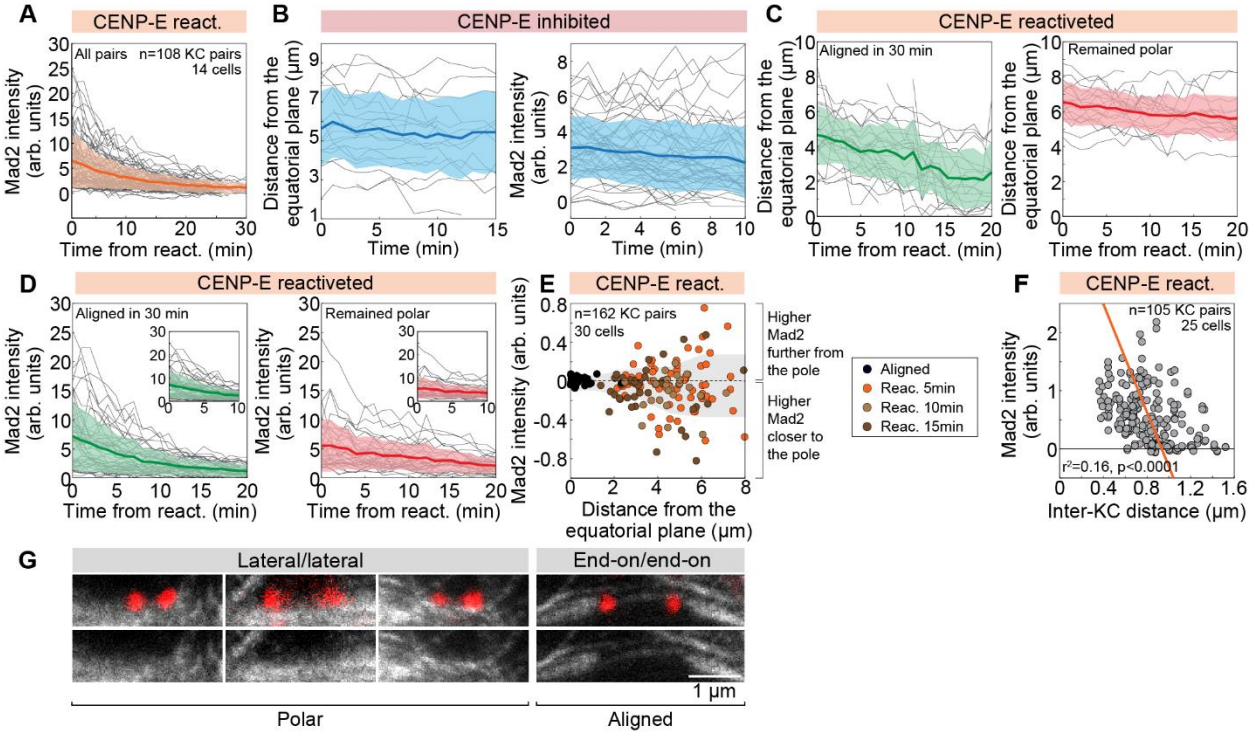

Figure S2. Mad2 signal on polar kinetochores drops gradually in time as a response to CENP-E reactivation prior to start of chromosome movement, related to Figure 2. (A) Mean Mad2 signal intensity of all polar sister kinetochore pairs in time from the washout of the CENP-E inhibitor. The thick black line represents the mean, and the purple area over the mean represents the standard deviation. (B) Distance of pairs of kinetochores from the equatorial plane (left) and mean Mad2 signal intensity (right) of pairs of polar sister kinetochores in time in the presence of the CENP-E inhibitor. (C, D) Distance from the equatorial plane (C) and mean Mad2 signal intensity (D) of polar kinetochore pairs in time from washout of the CENP-E inhibitor for kinetochore pairs that aligned in the 30-min period (green, left parts) and pairs that did not align in the same period (red, right parts). (E) Distance of kinetochore pairs from the equatorial plane versus difference in Mad2 levels between two sister kinetochores based on proximity of each kinetochore in a pair to the nearest pole in conditions depicted on the right. (F) Interkinetochore (Inter-KC) distance of sister kinetochore pairs versus mean Mad2 signal intensity of sister kinetochore pairs and linear regression (line). (G) Insets of kinetochore pairs with microtubules from different attachment categories as depicted imaged by STED microscopy (top) and schemes of microtubules (white) and kinetochores (red) of the respective insets (bottom). KC, kinetochore, inh., inhibition, reac., reactivated, arb., arbitrarily.

Supplementary Figure 3

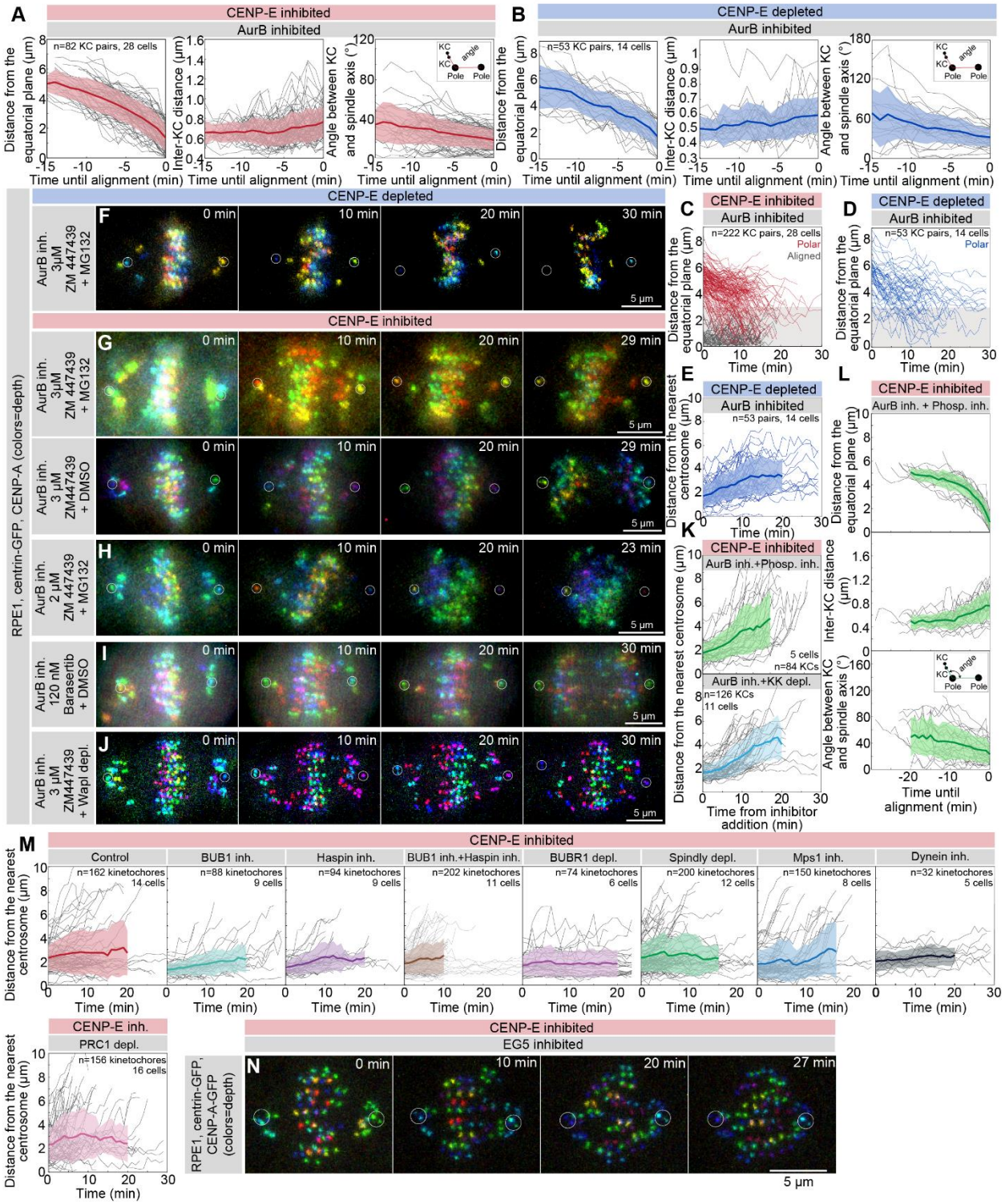

Figure S3. Chromosome congression in the absence of CENP-E is limited mainly by the outer kinetochore pool of Aurora B, related to Figure 3. (A, B) Distance to the equatorial plane of sister kinetochore pairs (left), interkinetochore (inter-KC) distance (middle) and angle between

sister kinetochores and main spindle axis as depicted on a scheme in top (right) in time until alignment of the kinetochore pair in cells after Aurora B was acutely inhibited by 3µM ZM447439 in already CENP-E inhibited condition (A) or in already CENP-E depleted cells (B). Thick lines represent means, and grey areas over means represent standard deviations. Centrioles are rounded by the white circle. (C, D) Distance to the equatorial plane of initially polar (red and blue) and initially aligned (black) sister kinetochore pairs in time from acute addition of 3µM Aurora B inhibitor ZM447439 in CENP-E inhibited cells (C) and CENP-E depleted cells (D), as indicated. (E) Distance to the nearest spindle pole of initially polar kinetochore pairs (blue) in time from acute addition of 3µM Aurora B inhibitor ZM447439 in CENP-E depleted cells. (F-J) Representative examples of RPE1 cells expressing CENP-A-GFP and centrin1-GFP in different frames following treatments: acute Aurora B inhibition by 3µM ZM447439 in cells depleted of CENP-E (F), acute Aurora B inhibition by 3µM ZM447439 in cells already treated with CENP-E inhibitor with (G top) and without (G bottom) addition of the 20µM proteasome inhibitor MG132, acute Aurora B inhibition by 2µM ZM447439 and MG132 in cells already treated with CENP-E inhibitor (H), acute Aurora B inhibition by 120 nM Barasertib and DMSO in cells already treated with CENP-E inhibitor (I), and acute Aurora B inhibition by 3µM ZM447439 and DMSO in cells depleted for 48h of WAPL and treated with CENP-E inhibitor (J). Images are maximum projections color coded by depth as specified by the color bar on figure 1A. Centrioles are rounded by the white circle. (K) Distance to the nearest centrosome of initially polar kinetochore pairs in time from the treatments indicated on top of each graph. (L) Distance to the equatorial plane of sister kinetochore pairs (top), interkinetochore (inter-KC) distance (middle) and angle between sister kinetochores and main spindle axis as depicted on a scheme in top (bottom) in time until alignment of kinetochore pairs in cells where both Aurora B by 3µM ZM447439 and phosphatases by 1µM Okadaic acid were acutely inhibited in the already CENP-E inhibited cells. (M) Distance to the nearest centrosome of initially polar kinetochore pairs in time from respective treatments indicated on top of each graph. (N) Representative example of RPE1 cell expressing CENP-A-GFP and centrin1-GFP in different frames as depicted after addition of 100µM Eg5 inhibitor monastrol in already CENP-E inhibited cells. Time represents the time from the acute treatment. KC, kinetochore, depl., depletion, inh., inhibition, react., reactivation, AurB, aurora B.

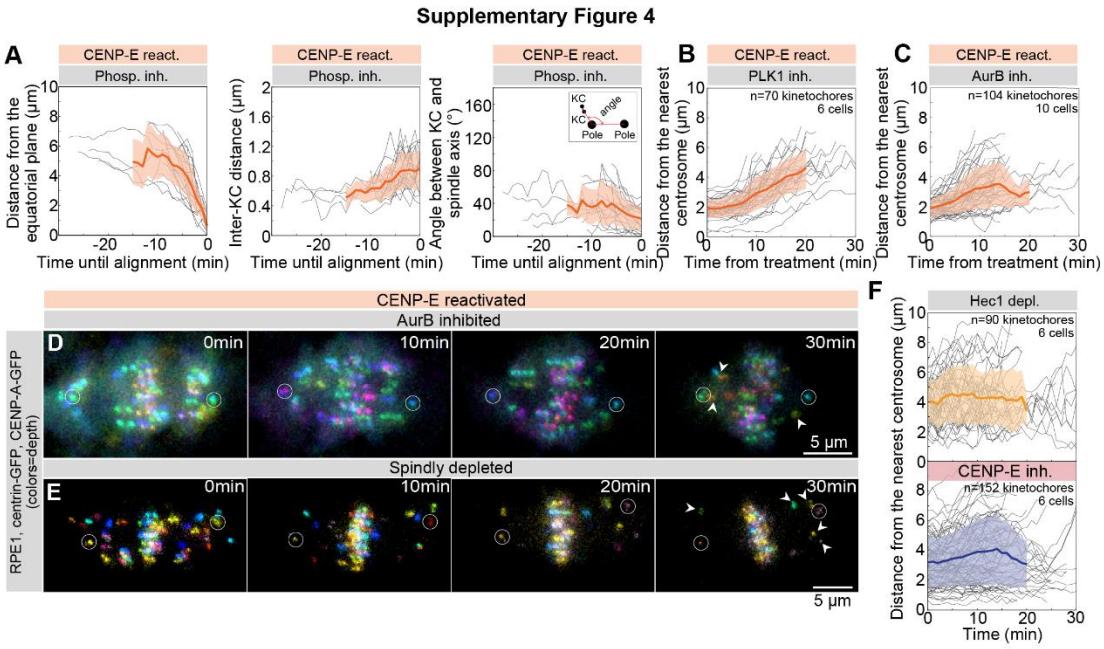

Figure S4. Chromosome congression after reactivation of CENP-E activity does not depend on protein phosphatases, related to Figure 3. (A) Distance to the equatorial plane of the sister kinetochore pairs (left), distance between sister kinetochores (middle) and the angle between sister kinetochores and the main spindle axis, as depicted on a scheme in the top (right) in time until alignment of the kinetochore pair in cells in which protein phosphatases were acutely inhibited by 1µM Okadaic acid treatment after wash-out of the CENP-E inhibitor. Thick lines represent means, and grey areas over means represent standard deviations. (B-C) Distance to the nearest centrosome of polar kinetochore pairs in time from the treatment indicated on top of each graph. (D-E) Representative examples of RPE1 cells expressing CENP-A-GFP and centrin1-GFP in different frames as depicted after wash-out of the CENP-E inhibitor and addition of 3µM Aurora B inhibitor ZM447439 (D) or wash-out of the CENP-E inhibitor in cells depleted of Spindly (E). Images are maximum projections color coded by depth as specified by the color bar on figure 1A. Time represents the time from the onset of acute treatment. (F) Distance to the nearest centrosome of initially polar kinetochore pairs in time from the treatments indicated on top of each graph. KC, kinetochore, inh., inhibition, AurB, aurora B, wash., washout.

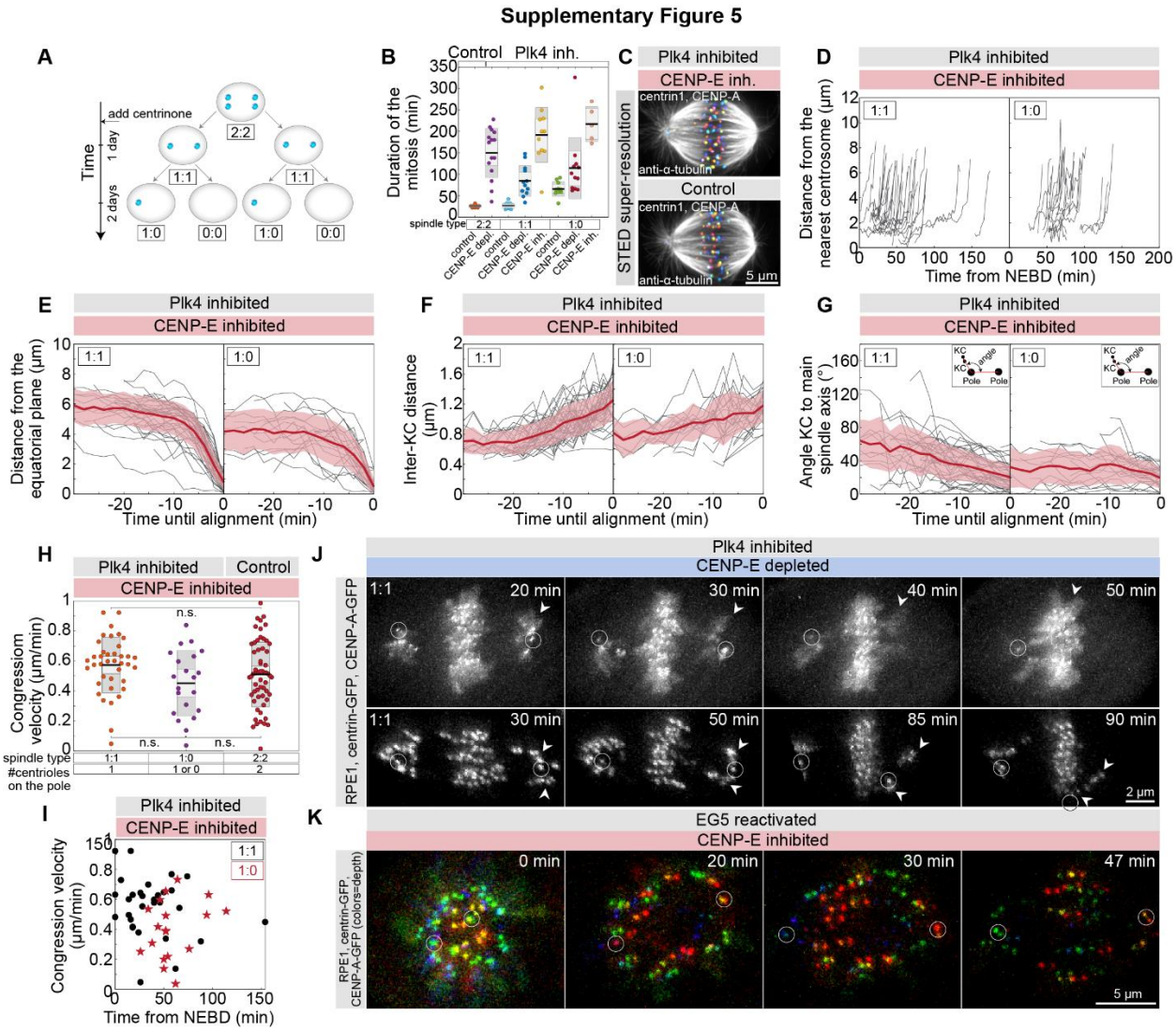

Figure S5. Various parameters of chromosome movement during congression are similar in cells with different numbers of centrioles, related to Figure 4. (A) Scheme depicting progressive centriole depletion in mitotic cells following continuous Plk4 inhibition by 300nM centrinone. (B) Duration of mitosis in cells with different number of centrioles after treatments indicated on bottom. The black line shows the mean; the light grey and dark grey areas mark the 95% confidence interval on the mean and standard deviation, respectively. (C-F) Distance from the nearest spindle pole in time from nuclear envelope breakdown (NEBD) of all initially polar kinetochore pairs (C), distance to the equatorial plane (D), interkinetochore (inter-KC) distance (E) and angle to the main spindle axis depicted on scheme in the graph (F) of a sister kinetochore pairs in time until alignment for initially polar kinetochores in the presence of the CENP-E inhibitor for cells with different number of centrioles as indicated in the top left part of each graph. Thick lines represent means, and pale areas over means represent standard deviations. (G) Velocity of chromosome congression during the 6-minute period that precedes complete alignment for depicted treatment in time from the onset of mitosis for cells with the number of centrioles as indicated. (H) Velocity of chromosome movement during the 6-minute period that precedes

complete alignment versus time from NEBD for each polar kinetochore pair. (I) Representative examples of RPE1 cells expressing CENP-A-GFP and centrin1-GFP in different frames from the onset of NEBD after depletion of CENP-E. Centrioles are rounded by the white circle. Arrowheads depict polar chromosomes that align after centriole separation from centrosome. K) Representative example of RPE1 cell expressing CENP-A-GFP and centrin1-GFP in different frames from the wash-out of the Eg5 inhibitor monastrol and acute inhibition of CENP-E by 80nM GSK923295. Time 0 represents the time of the wash-out of monastrol and the addition of the GSK923295. KC, kinetochore, inh., inhibition.

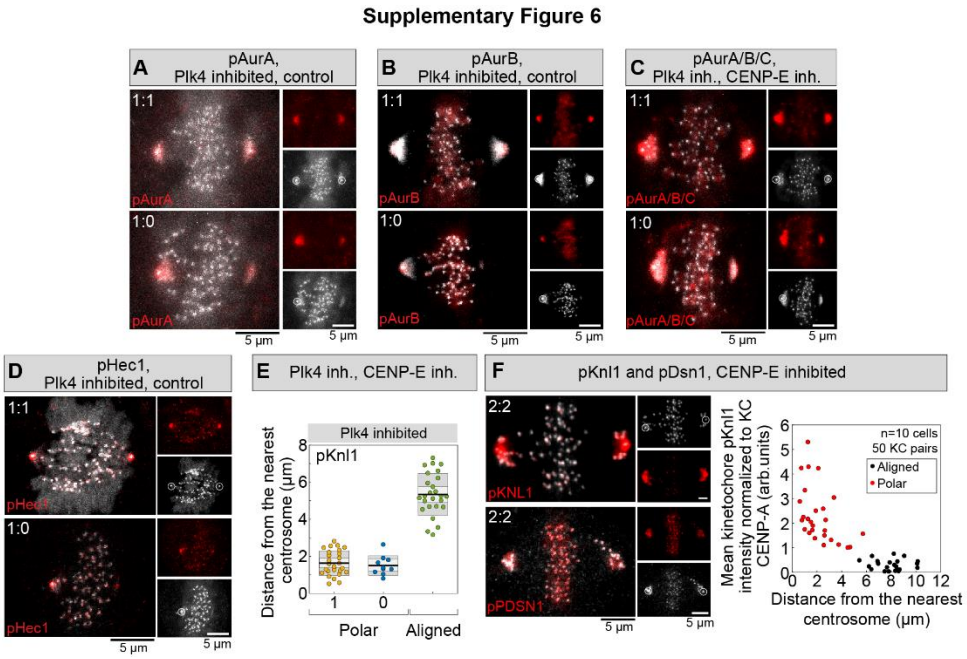

Figure S6. Aurora-B mediated phosphorylation declines gradually on outer-kinetochore substrates as polar chromosomes congress to the metaphase plate, related to Figure 5. (A-D) Representative examples (left) and separated channels (right) of RPE-1 cells expressing CENP-A-GFP and centrin1-GFP immunostained with antibodies targeting phosphorylated residues of indicated proteins (pAurA, pAurB, pAurA/B/C and pHec1) with different numbers of centrioles on each spindle pole after 300nM centrinone treatment as depicted for control cells treated with DMSO as indicated on top. The images are maximum projections. (E) Distance from a spindle pole of different group of kinetochores as indicated on bottom. (F) Representative examples and separated channels on right of RPE-1 cells expressing CENP-A-GFP and centrin1-GFP immunostained with antibodies targeting phosphorylated residues of pKnl1 (top left) and pDsn1 (bottom left) after inhibition of CENP-E activity (left) and plot of mean signal intensity of pKnl1 on polar and aligned kinetochore pairs versus distance of pairs from the spindle pole. n.s., nonsignificant. Statistics: One-way ANOVA. Inh., inhibited, depl., depleted, chr., chromosomes.

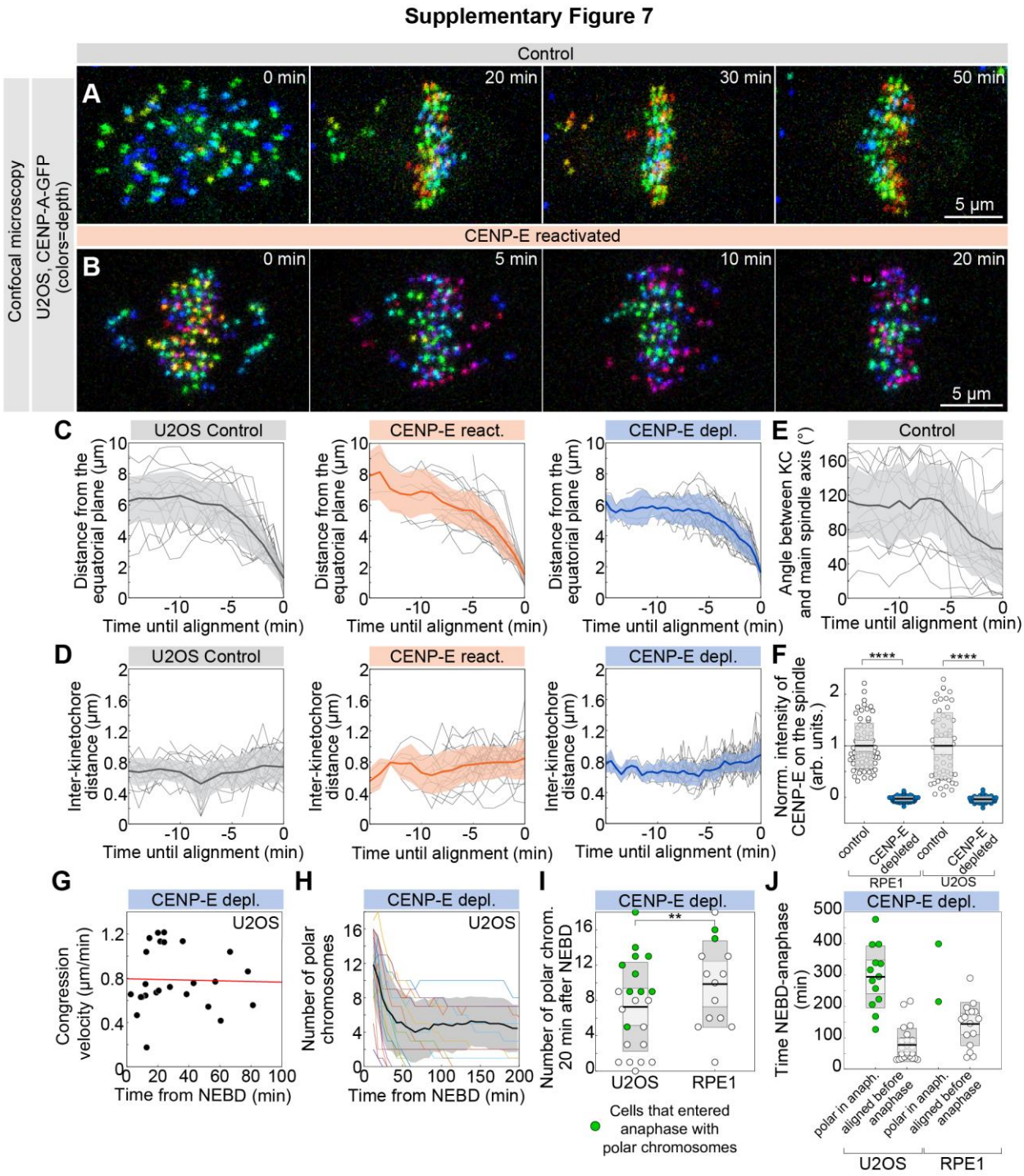

Figure S7. Various parameters of chromosome movement during congression are similar in cells with and without CENP-E activity in the U-2 OS cancer cell line, but congression often fails in U-2 OS cells in the absence of CENP-E activity, related to Figure 6. (A, B) Representative examples of a U-2 OS cells expressing CENP-A-GFP imaged by confocal microscopy in different frames as depicted in control DMSO condition (top) and after wash-out of the CENP-E inhibitor 200 nM GSK923295. Time 0 represents onset of nuclear envelope

breakdown (NEBD) (A) or wash-out (B). The image is a maximum projection color coded by depth as specified by the color bar on figure 1A. (C-E) Distance of polar kinetochores to equatorial plate of the spindle (C), and interkinetochore (inter-KC) distance (D), and the angle between sister kinetochores and main spindle axis as depicted on scheme in the graph (E) in time until alignment of kinetochore pair across treatments indicated on top of each graph. (F) Velocity of chromosome congression during last 4 minutes before polar chromosome aligned to the equatorial plane versus time from NEBD for each polar pair and regression (line). (G) Relative intensity of CENP-E on the spindle after immunofluorescence in control cells treated with non-targeting siRNA and in CENP-E depleted cells treated with CENP-E siRNA for both RPE-1 and U2OS cells, as indicated. The mean signal I each cell line is normalized to mean value in control population. (H) Number of polar chromosomes in time from NEBD in U-2 OS cells after 48h of depletion of CENP-E. Different cells are represented by different colours. Thick lines represent means, and grey areas over means represent standard deviations. (I) Time from NEBD to anaphase onset for indicated mitotic outcomes in U-2 OS and RPE-1 cell lines after CENP-E depletion. The black line shows the mean; the light grey and dark grey areas mark the 95% confidence interval on the mean and standard deviation, respectively. (J) Number of polar chromosomes 20 minutes after NEBD in U-2 OS and RPE-1 cells depleted of CENP-E. Green squares on (H) and (I) represent cells that eventually entered anaphase with polar chromosomes. depl., depletion, inh., inhibition, react., reactivation.

SUPPLEMENTARY VIDEO CAPTIONS

Video 1. Lattice-light sheet microscopy (LLSM)-based assay for large-scale live cell imaging. Dozens of RPE-1 cells stably expressing CENP-A-GFP and Centrin1-GFP (16-colors) in control cells treated with DMSO, imaged by LLSM right after addition of the drug. Kinetochores and centrioles are color-coded for depth from blue to red with the 16 Colors LUT.

Video 2. RPE1 cells stably expressing CENP-A-GFP and Centrin1-GFP in control and CENP-E reactivated conditions, imaged by LLSM. RPE-1 cells stably expressing CENP-A-GFP and Centrin1-GFP (16-colors LUT) in cells treated with DMSO (control, left) and after wash-out of the CENP-E inhibitor (CENP-E reactivated, right). Cells were imaged right after drug addition (left) or right after drug wash-out (right). Kinetochores and centrioles are color-coded for depth from blue to red with the 16 Colors LUT.

Video 3. RPE1 cells stably expressing CENP-A-GFP and Centrin1-GFP in CENP-E depleted and CENP-E inhibited conditions, imaged by LLSM. RPE-1 cells stably expressing CENP-A-GFP and Centrin1-GFP (16-colors LUT) in cells treated with CENP-E siRNA for 48h (CENP-E depleted, left), and with CENP-E inhibitor (CENP-E inhibited, right). Cells were imaged 48h after addition of CENP-E siRNA (left) or 3h after the addition of the CENP-E inhibitor (right). Kinetochores and centrioles are color-coded for depth from blue to red with the 16 Colors LUT.

Video 4. RPE1 cells stably expressing CENP-A-mCerulean and Mad2-mRuby following reactivation of CENP-E activity, imaged by confocal microscopy. RPE-1 cell stably expressing CENP-A-mCerulean (grey) and Mad2-mRuby (red) in cells treated with CENP-E inhibitor for 3h followed by drug wash-out. Cells were imaged right after wash-out of the drug. Scale bar, 5 µm.

Video 5. RPE1 cells stably expressing CENP-A-GFP and Centrin1-GFP in CENP-E inhibited condition following addition of inhibitors of Aurora kinases, and in CENP-E reactivated condition following depletion of BubR1 and addition of inhibitor of phosphatases, imaged by confocal microscopy. RPE-1 cells stably expressing CENP-A-GFP and Centrin1-GFP (16-colors LUT) in cells treated with CENP-E inhibitor for 3h followed by acute inhibition of Aurora B kinase (top left), acute inhibition of Aurora A kinase (top right), and in cells treated with CENP-E inhibitor for 3h followed by wash-out of the drug in cells depleted for BubR1 (bottom left), and cells acutely treated by phosphatases inhibitor (bottom right). Cells were imaged right after addition of the last drug or drug wash-out. Kinetochores and centrioles are color-coded for depth from blue to red with the 16 Colors LUT and noise was processed with the Despeckle function in ImageJ.

Video 6. RPE1 cells stably expressing CENP-A-GFP and Centrin1-GFP in Plk4-inhibited cells with different number of centrioles in CENP-E inhibited and CENP-E depleted conditions imaged by confocal microscopy. RPE-1 cells stably expressing CENP-A-GFP and Centrin1-GFP (16-colors LUT) in cells treated with Plk4 inhibitor for 2 days with distinct number of centrioles on each centrosome (1:1, 1:0, and 0:0) and subsequently treated with CENP-E inhibitor for 3hr before imaging (CENP-E inhibited, left) and with CENP-E siRNA for 48hr before imaging (CENP-E depleted, right). Cells were imaged 48h after addition of CENP-E siRNA (left)

or 3h after the addition of the drug (right). Kinetochores are color-coded for depth from blue to red with the 16 Colors LUT.

Video 7. U2OS cells stably expressing CENP-A-GFP following CENP-E depletion imaged by LLSM. U2OS cells stably expressing CENP-A-GFP (grey) following treatment with CENP-E siRNA for 48h. Cells were imaged 48h after addition of CENP-E siRNA. The noise was processed with the Despeckle function in ImageJ. Scale bar, 5 µm.